1

Introduction and Fundamentals of Mixed-Valence Chemistry

Chun Y. Liu and Miao Meng

Jinan University, College of Chemistry and Materials Science, Department of Chemistry, 601 Huang-Pu Avenue West, Guangzhou 510632, China

1.1 Introduction

The term mixed valence (MV) is used to describe chemical systems in condensed media and solids in which the same chemical element exists in different oxidation states [1–3]. Thus, MV compounds refer to the category of unimolecular systems consisting of more than one redox center derived from the same element but formally having different oxidation levels in the ground state. In this context, molecules or solids having the same chemical constitutions but different oxidation states for the nonequivalent atoms should be viewed as distinct chemical identities or materials, but those having the same oxidation level are chemically identical. Prussian blue, the prototype of MV compound, is identical to Turnbull's blue [4]. It should be addressed that in MV compounds, the oxidation states of individual redox-active atoms that share the same elemental redox potential depend upon the electronic properties of the chemically bonded atoms or groups. For example, a high oxidation level is given to a redox center surrounded by more or stronger electron-withdrawing atoms or groups, and vice versa, a lesson learned from text book chemistry. However, mixed valency of MV compounds, which concerns charge distribution over the molecular ground state, is a very comprehensive issue pertaining to electrons and nuclei in motion that compasses a number of fundamental chemical problems, including energetic, dynamic, kinetic, and mechanistic of chemical transformations [5–8]. Moreover, MV compounds possess a unique optical property resulting from charge transfer between the spatially separated (chemically bonded or nonbonded) atoms with different valence electron shells. The interplays of electronic and nuclear dynamics within the molecule and between molecules (MV molecules and solvent molecules) are implicated through their optical behaviors, which are translated into the dynamics and energetics of the interpenetrated chemical and physical systems. With its enriched scientific contents, mixed-valent chemistry has evolved into one of the major playgrounds in modern chemistry in its own right for experimental and theoretical practitioners [6–10].

Mixed-Valence Systems: Fundamentals, Synthesis, Electron Transfer, and Applications, First Edition. Edited by Yu-Wu Zhong, Chun Y. Liu, and Jeffrey R. Reimers.

The attraction of mixed-valence systems is largely enforced by the fact that the valences of the discrete redox centers are intramolecularly self-exchangeable, thus representing the most elementary chemical reaction: intramolecular electron transfer (ET). In the middle of last century, the theoretical framework for ET was constructed and expanding rapidly, as marked by a series of profound progresses made in a relatively short period of time. Kubo and Toyozawa derived the general expression of activation energy (1955) [11]; Levich and Dogonadze presented the rate equation for ET reaction in the nonadiabatic limit (1960) [12, 13]; Marcus introduced the dielectric continuum model of solvation and the classical ET kinetic formalism (1956) [14, 15]; McConnell developed the superexchange model (1961) [16]; and Hush described the intramolecular effects using coupled harmonic surfaces (1958) [17] and calculations of the electronic coupling integral from intervalence optical parameters (1967) [5]. In the two-state description, the energy profiles of initial and final states of the system are approximated with a harmonic oscillator, which models the incorporated electron–nuclei dynamics in chemical transformation from reactant to product along the reaction coordinate. This simplified theoretical model on ET demands an experimental model that has single transferring electrons and well-defined electronic configuration. Thus, research work on MV chemistry gained a strong impetus to experimentally monitor the ET processes and to validate the semiclassical theories.

The follow-up experimental study was pioneered by Taube and Creutz with the elegantly designed, pyrazine (pz)-bridged diruthenium complex (**I**), $\{[(Ru(NH_3)_5](\mu\text{-pz})[(Ru(NH_3)_5]\}^{5+}$, known as the Creutz–Taube ion [18], in which the two bridged Ru ions have formal oxidation numbers +2 and +3.

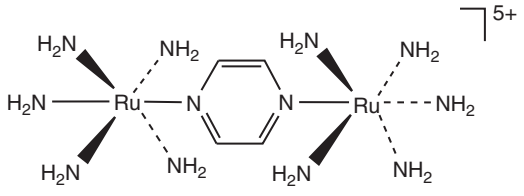

I

In a formal sense, the $Ru^{2+}(d^6)$ and $Ru^{3+}(d^5)$ centers in **I** serve the electronic donor (D) and acceptor (A), respectively, and electron self-exchange crossing the pz bridge (B) occurs without change of the free energy ($\Delta G = 0$). In the mixed-valent D–B–A molecular system, electron migrating from D to A and nuclear motion conform energetically and dynamically to the semiclassical two-state models [19, 20]. The Creutz–Taube ion allowed the first observation of Frank–Condon transition that induces ET between two metal centers in a molecular complex, namely, intervalence charge transfer or IVCT [18, 21]. Inspired by the Creutz–Taube complex, a large number of MV compounds in form of D–B–A with various transition metal complex and organic charge-bearing units for the D and A sites have been synthesized, and studied in terms of electronic coupling (EC) and ET [6, 8, 22–24].

Electron transfer in MV systems may proceed via one of the two reaction pathways, thermal or optical [6, 22, 25–27]. By thermal ET pathway, the system overcomes the thermal energy barrier (ΔG^*) and reaches the transition state through thermal fluctuations. In the transition state, designated as $[D–B–A]^{\neq}$ and $[A–B–D]^{\neq}$ in Figure 1.1 for the forward and reverse reactions, respectively, the system has an averaged nuclear configuration for the MV molecule (the activated complex) and solvation. From the reactant to the product, the system experiences an adiabatic process. Optical ET in MV compounds is initiated by vertical transition of the reactant state (with the extra electron on the donor) to the vibrational excited states of the product (with the extra electron transferred to the acceptor) (Figure 1.1). This transition occurs between two diabatic states and is governed by the Frank–Condon principle. Radiationless relaxation of the system from the nuclear excited state to the ground states completes the ET process [6, 19, 25].

For the ET event to occur, no matter which pathway is taken, the donor and acceptor electronic states must be coupled. It is the extent of coupling that controls the ET dynamics and kinetics, which is quantified by the coupling matrix element in quantum mechanics, i.e. H_{ab}. Hush demonstrated that this crucial quantity can be derived from the IVCT spectrum of the MV compound [5, 6, 9, 19]. The Hush model connects the spectral data (transition energy, intensity, and absorption bandwidth) of the molecular system and the energetic parameters of the ET reaction (coupling integral and thermal ET barrier), and paves the way to optical determination of ET rate constant (k_{ET}). This optically determined coupling integral (H_{ab}) can be incorporated into adiabatic and nonadiabatic ET kinetic expressions in the classical and semiclassical formalisms, which have been successfully applied in strongly and weakly coupled MV systems, respectively. Advances in time-resolved spectroscopic techniques allow the photoexcited states to be monitored, thus providing a powerful means for study of the photoinduced ET process in systems involving electronic excited states, D*–B–A or D–B–A*. Optical study of MV compounds and transient spectroscopic investigations of photoinitiated ET are complemented in development, validation, and refinement of the contemporary ET theories [19, 20, 25]. The gained

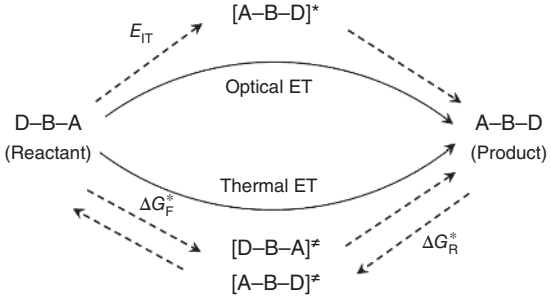

Figure 1.1 Optical (top) and thermal (bottom) ET pathways in mixed-valence D–B–A compounds. [A–B–D]* represents the vibrational excited state of the product. E_{IT} is the intervalence charge transfer transition energy. $[D–B–A]^{\neq}$ and $[A–B–D]^{\neq}$ refers to the transition complex for the reactant and product, respectively. ΔG^*_F and ΔG^*_R is activation energy of the forward and reverse ET reaction, respectively.

understanding allows control of electron (charge) transfer in molecular systems and elucidation of the long-range charge transport processes in biological system and is beneficial to development of innovative technologies such as conductive materials, molecular electronics, and catalysts for solar–chemical energy conversion.

1.2 Brief History

Historically, mixed-valence solids were found several centuries ago in various minerals, such as metal oxides, sulfates, and phosphates, in which the metal elements exist in different valence states [1, 3, 28]. These minerals usually show intense colors. The coloration of vivianite crystal with the chemical formula $Fe_3(PO_4)_2 \cdot 8H_2O$ is one of the interesting examples [5]. Vivianite is colorless when freshly exposed, as expected for the Fe^{2+} ion; after being exposed to air, it shows varying colors from light blue, light green, to dark blue or green, depending on the length of exposure due to oxidation of Fe^{2+} to Fe^{3+}. As early as in the eighteenth century, it was realized that the blue color of ceramic glaze on vases was produced from ferrous iron (Fe^{3+}) in reducing conditions. In nearly the same period of time, Prussian blue became a popular pigment for artists, which contains Fe^{3+} ions and negatively charged hexacyanoferrate ions $[Fe(CN)_6]^{4-}$, formulated as $Fe_4[Fe(CN)_6]_3$, as described in the chemistry text book at entry level. However, chemists at that time were unable to explain the coloration of this material because both ferrous and ferric ions in aqueous solution do not show strong absorptions in this particular spectral range. It was generally observed that solutions or solids containing an element in two different valence states often exhibit unusual intense coloration, which does not appear when either of the elements is present alone [3]. This recognition connected coloration of the complexes to the valences of its ingredients [1], importantly, beginning to be aware that the distribution of oxidation states within the molecule can exchange under the influence of light so as to produce the light absorption and hence the color. For these systems, "valency oscillation" and "resonant valency" were proposed to describe the physical origin of intense color presented by one element in different valence states [29], which is more or less close to today's understanding. In 1950s, long-distance electron transfer between metal ions was assumed to explain "valency oscillation." Weyl first noted that light absorption in MV systems is related to the interactions between two valence states of the same element [30].

Mixed-valence phenomena are also widely seen in enzymes and cofactors of biological systems where the active sites consist of multiple metal centers in variable oxidization states. For example, naturally occurring photosynthesis produces energy materials from low-potential molecules such as H_2O and CO_2 by absorption of visible light. The energy conversion processes involve two protein cofactor complexes, namely, photosystems (PS) II and I. In PS II, the oxygen-evolving complex (OEC), which conducts oxidation of water to molecular oxygen, is an ox-tetramanganese cluster with the Mn atoms in different oxidation levels [31]. In PS I, ferredoxin $\{(Cys)_2Fe^{II}\text{-}(\mu\text{-}S)2Fe^{III}(Cys)_2\}^+$ ([2Fe2S]) is the electron carrier that transports electrons to the enzymatic reductive reaction

center, the ferredoxin([2Fe2S])-nicotinamide adenine dinucleotide (NADP/H) reductase (FNR) [32]. Accomplishments of these biochemical reactions depend on intramolecular and intermolecular electron transfer with the driving force ultimately from sunlight [33].

In 1960–1970s, three important publications by Hush (1967) [5], Robin and Day (1968) [34], and Creutz and Taube (1969) [35] marked the cornerstone in development of mixed-valence chemistry. Based on the Mulliken charge transfer theory, Hush demonstrated [36, 37] that the electronic coupling matrix element (H_{ab}) can be calculated from the IVCT parameters [5–7], transition energy E_{IT}, molar extinction coefficient ε_{IT}, and half-height bandwidth $\Delta\nu_{1/2}$ (Eq. 1.1).

$$H_{ab} = 2.06 \times 10^{-2} \frac{(E_{IT}\varepsilon_{IT}\Delta\upsilon_{1/2})^{1/2}}{r_{ab}} \tag{1.1}$$

where E_{IT} and $\Delta\nu_{1/2}$ are in wavenumber (cm^{-1}) and r_{ab} is the effective electron transfer distance in angstrom (Å). This Mulliken–Hush expression, developed in the pure classical two-state regime, can be used in broad range of double-well charge transfer systems. The Hush model also reveals the correlation between optical (radiative) and thermal (radiationless) electron transfer for symmetric MV systems [5, 7, 14, 38].

$$E_{IT} = 4\Delta G^{*} \tag{1.2}$$

Equation (1.2) suggests that the kinetics and energetics for the ET process can be described through optical analysis of the intervalence charge transition of MV compounds [19]. It is interesting that this fundamental energetic relationship concerning activation energy of ET reaction was revealed by Kubo and Toyozawa [11], Marcus [14], and Hush [5] from their independent works.

Robin and Day provided a scheme that classifies the MV compounds in terms of the extent of electronic coupling [34]. According to them, within the semiclassical framework, there are three regimes that MV compounds in different coupling strength belong to, that is, noncoupled (fully localized) Class I, strongly coupled or fully delocalized Class III, and the intermediate Class II that encompasses systems from weakly to moderately strongly coupled. In Robin–Day's classification [34], for MV compounds in Class I, thermal exchange of the oxidation states for the element in different sites is very slow, and the optical transition occurs by weak absorption of high-energy photons, while in Class III compounds, the valence states for the element in the multiple sites are averaged and thus crystallographically indistinguishable [1]. Class II compounds are those for which the electronic wave functions of the ground state and the excited state are significantly mixed, and the valence states are interchangeable in response to external stimulations, such as light and heat [1, 34].

Synthesis of the Creutz–Taube complex in 1969 initiated experimental studies of intramolecular EC and ET. For the Creutz–Taube ion, a broad, asymmetric absorption band was observed at 6369 cm^{-1}, which was attributed to electron transfer from Ru^{2+} to Ru^{3+} crossing the pyrazine molecule. However, it took many years to characterize this MV compound in terms of the Robin–Day's scheme, that is, whether

it belongs to localized Class II with +2 for one Ru center and +3 for the other or to delocalized Class III with an averaged oxidation state of +2.5 for each of the two Ru centers. Now, it is generally accepted that the Creutz–Taube ion is best placed on the Class II–III borderline [39, 40].

A prominent feature of MV compounds is the observation of characteristic IVCT transition that occurs in a broad region from visible to infrared depending on the strength of electronic coupling between the redox centers. By analyzing the IVCT band, important parameters of the ET process between mixed-valent redox sites can be extracted, including the reorganization energy (λ), the electronic coupling parameter (H_{ab}), and the thermal activation barrier (ΔG^*). These concepts arose from the seminal works of Kubo and Toyozawa, Marcus, and Hush concerning the activation energy, Marcus and Hush regarding the intermolecular and intramolecular contributions to the reorganization energy, and Hush and Levich and Dogonadze to the electronic coupling [12, 41]. McConnell's theory is then applied to understand the dependence of the coupling, and hence the spectra, on systematic extension of the separation between the mixed-valence centers. These pioneering works established the theoretic framework of mixed-valence chemistry, which has inspired and guided research in this field for a half century [1, 2, 6, 8].

1.3 Diversity of Mixed-Valence Systems – Some Examples

Following the Creutz–Taube ion, various mixed-valence D–B–A compounds were synthesized with different $d^{5\text{-}6}$ transition metal ions (Ru, Os, and Fe) by substituting the auxiliary ligands NH_3 with inorganic anions, e.g. Cl^-, CN^-, or organic molecules, e.g. bipyridine (bpy) and terpyridine (tpy), or by modifying the bridging ligand (BL) [6, 8, 40]. For these analogues, broad, low-energy IVCT absorptions are observed typically in the near-infrared region. Asymmetrical compounds derived from heterodinuclear metal centers [42], or from homodinuclear metal ions coordinatively saturated with different supporting ligands [43], exhibited distinct energetic profiles in the two-state framework, i.e. $\Delta G^0 \neq 0$, and attracted significant attention. However, for dinuclear $d^{5\text{-}6}$ systems with building blocks that have distorted octahedral geometry, the intervalence spectrum must be carefully assigned because the d orbitals between the two metal centers interact through dπ–dπ conjugations across BL [39, 40]. As a result, multiple electronic transitions, including three intervalence transitions (IT) and two interconfigurational (IC) transitions occurring at the acceptor, may appear, as shown in Figure 1.2, and may overlap with each other [40]. In this case, only the lowest energy IT band, IT(1) in Figure 1.2, arises from pure donor–acceptor ET that accounts for the reorganization energy (λ) [39].

When multidentate pyridyl and phenyl ligands are used, the degeneracy of d orbitals in an octahedral field is removed, which gives rise to single intervalence band for the mixed-valence complexes. Organometallic Ru (II/III) building blocks prepared with multidentate phenyl ligands feature five-membered ring structures

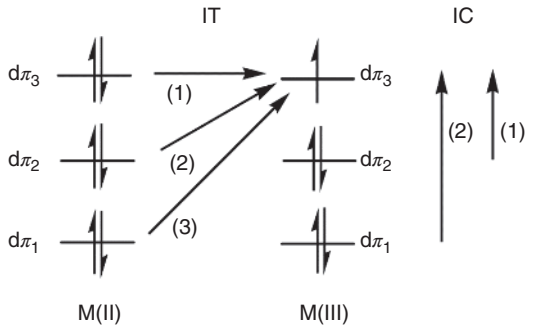

Figure 1.2 Multiple transitions occurring in d^{5-6} mixed-valence M–BL–M systems (M = Ru and Os).

involving a Ru—C bond (**II**). The cyclometalated Ru redox centers are able to increase the molecular rigidity and stability of the assembled D–B–A complexes and to strengthen the d(Ru)–π(phenyl ligand) orbital interactions [44]. Aligning the Ru—C bonds on the donor and acceptor sites with the IVCT axis substantially enhances the electronic coupling by favoring the BL-mediated hole transfer pathway [45].

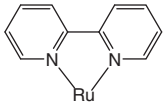

bpy

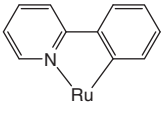

IIa

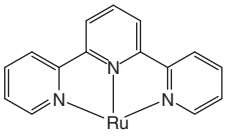

terpy

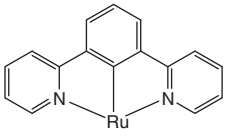

IIb

The first reported dinuclear MV complex with nonoctahedral redox sites was the biferrocenium cation $[(C_5H_5)Fe\text{-}(C_5H_4\text{-}C_5H_4)\text{-}Fe(C_5H_5)]^+$ (**III**), synthesized by Cowan and coworkers in 1973 [46]. This molecule exhibits a broad IVCT band at 1900 nm. With different BLs, a series of ferrocenium MV organometallics have been studied in terms of electronic coupling [47]. In earlier studies, few other transition metals were used to construct binuclear MV systems. For example, transition metal ions in group VIB of the periodic table were exploited as the redox centers, typically, $[M(CO)_3(PR_3)_2]_2(\mu\text{-pz})$ (M = Mo and W) (**IV**) [48, 49] and $[Mo(tp^*)(NO)Cl]_2(\mu\text{-BL})]$ (tp^* = tris(3,5-dimethylpyrazolyl)hydroborate) (**V**) [50]. These dinuclear organometallic complexes feature an $18\,e^-$ configuration for each metal center and present redox properties sensitive to the coordination environment due to the strong π back-bonding from the ligand to the metal center [51]. $\{[Mo(CO)_3(PR_3)_2]_2(\mu\text{-pz})\}^+$ with an electronic configuration $4d^5/4d^6$ exhibits a relatively narrow ($\Delta\nu_{1/2}$ 700 cm^{-1}), symmetric IVCT band (4650 cm^{-1}) in the near-IR region [49].

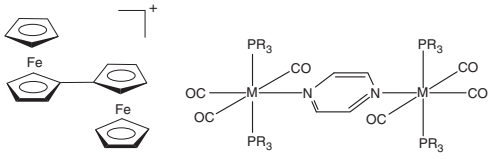

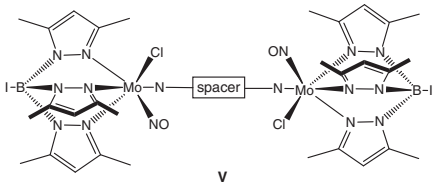

In the 1990s, unimolecular mixed-valence D–B–A systems were extended from metal-containing inorganic complexes to pure organic compounds. The bistriarylamine (**VI**) [52, 53] and bishydrazine (**VII**) [54, 55] derivatives involving redox-active sp^3 nitrogen atoms are the prototypes of organic MV D–B–A systems, which were studied systematically by Nelsen and Lambert, respectively. Following these works, another organic radical system, namely, $D–BL–D^{\bullet+}$ (**VIII**), was developed in Kochi's group, with a redox-active group 2,5-dimethoxy-4-methylphenyl (D) as the donor and acceptor [56]. By employing redox-active organic groups, the concepts of mixed-valence chemistry are generalized. Compared to metal complex systems, the organic systems possess several features that favor study of EC. In these radical systems, electronic coupling and electron transfer involve single electrons that are specified with respect to orbital and electronic state, which facilitates the assignment and analysis of the IVCT bands. Study of organic systems concerns all aspects of mixed-valence chemistry, which has contributed to advance our knowledge in this field [24, 57].

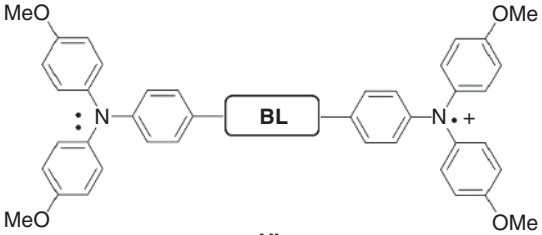

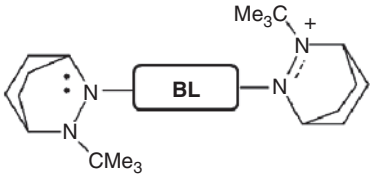

VII

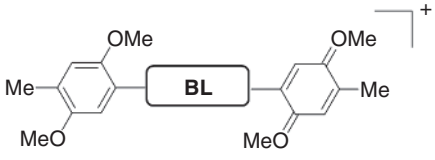

VIII

The family of bridged MV compounds was further expanded with involvement of redox-active metal clusters containing more than one metal atom, used as a whole to be a building block for assembling the D–B–A molecule. Linking two quadruply-bonded dimetal units, M_2 (M = Mo and W), with a tetradentate bridging ligand was first achieved in Chisolm's group in 1989 [58], yielding the *dimers of dimers* of form of M_2–BL–M_2, which has a formal oxidation state +4 for each of the M_2 centers, as shown in **IX**. The MV complexes $[M_2–BL–M_2]^+$ are prepared by one-electron oxidation using appropriate oxidizing reagents [58, 59]. Cotton and coworkers optimized the synthetic method with the designed dimolybdenum building block $[Mo_2(DAniF)_3]^+$ (DAniF = *N*,*N*′-di(*p*-anisyl)formamidinate) for converged assembly [60, 61], which led to the synthesis and structural characterization of many Mo_2 dimers with diverse bridging ligands. A quadruply-bonded M_2 unit has a well-defined, distinct electronic configuration, $\sigma^2\pi^4\delta^2$ [62]. For this M_2 MV complex system, electron delocalization within the M_2 unit is assumed. In a view of electron localization, the donor site (M_2^{4+}) has a close shell with the valence electrons paired in the δ orbital, while in the acceptor (M_2^{5+}), the δ orbital is singly occupied. Therefore, in the M_2 dimers, EC and ET involve only the δ electrons. Recently, Liu and coworkers systematically studied EC and ET in the Mo_2 MV systems under the contemporary ET theories [63, 64]. Covalently bonded diruthenium complexes were exploited by Ren and coworkers as the redox centers to assemble Ru_2 dimers through an axial linkage. For the Ru_2–BL–Ru_2 systems, polyyn-diyl chains –$(C_2)_n$– are the favorable bridging ligands to link two $Ru_2(ap)_4$ (ap = 2-anilinopyridinate) complex molecules (**X**) with the number of alkynyl units (n) up to 6 [65].

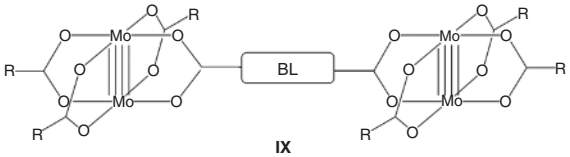

IX

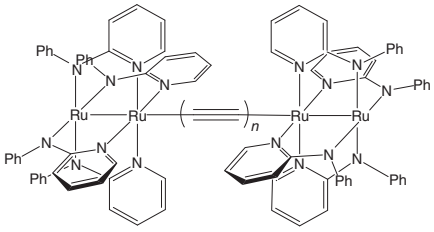

X

The oxygen (O)-centered triruthenium cluster, $[Ru_3O(acetate)_6\text{-}(CO)L_2]$, has been used as the electron donor or acceptor for construction of the MV D–B–A complexes by Ito and Kubiak [66]. In a $[Ru_3O(acetate)_6\text{-}(CO)L_2]$ complex, the three Ru atoms are in formal oxidation states III, III, and II, which presumably are fully delocalized through the acetate bridging ligands. Replacing one of the L ligands with a pyridyl ligand modifies the redox potential of the Ru_3 center, which controls the properties of donor and acceptor; the other L position is replaced by a pyridyl bridging ligand, resulting in the *dimer of trimers* (**XI**). The mixed-valence system results from one-electron reduction of the Ru_3 dimers, $\{Ru_3(III, II, II)–BL–Ru_3(III, III, II)\}^-$. In this system, the electronic coupling can be tuned by alternation of the remaining L ligand, besides variation of the BL. Uniquely, the CO groups function as an IR probe, which has been successfully used to study the ET kinetics by analysis of vibrational band broadening of the carbonyl group [66, 67].

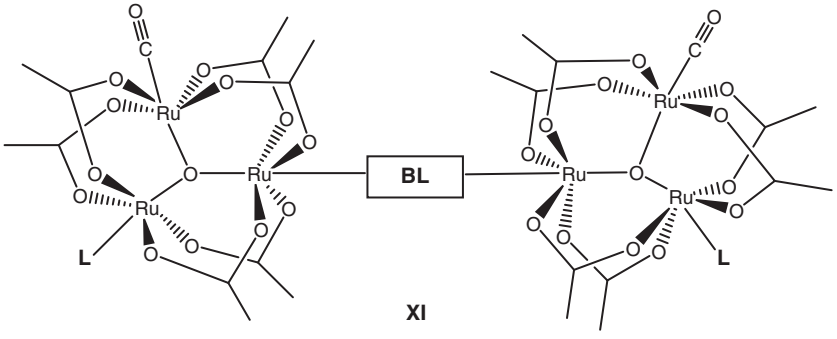

XI

It is generally recognized that in MV D–B–A molecules, the bridging ligand plays a dominant role in control of D–A electron transfer. For decades, much of the work has focused on BL mediation of electronic coupling [23, 24, 47, 68]. In these studies, the main goals are to evaluate efficiency of various BL in coupling the

electronic states, to determine its ability of transporting electrons, and to explore how the electronic event takes place. The study encompasses three crucial aspects of electron transfer reactions: energetics, kinetics, and mechanism. Approaches to these issues include variation of the BL structures, mainly through changes in length, conformation, and conjugation. Distance dependence of EC is the characteristic property for a given MV system [69], determined by the nature of the donor and acceptor. For a homologous series with varying BL length, the distance dependence of EC and ET can be evaluated by an attenuation factor β, which describes the exponential decay of EC constant (H_{ab}) or ET rate (k_{et}) against charge transfer distance (r_{ab}) [47, 69]. For a D–B–A series specified with the same D and A units, the magnitude of β reflects the charge transport ability of the BL type, and it is generally realized that a conjugated BL gives a small β value compared to saturated and cross-conjugated BLs. The influence of BL geometric conformation on EC has been intensively investigated in both inorganic [70] and organic MV systems [24, 71, 72]. On this issue, understanding obtained from combined experimental and theoretic work has revealed that BL conformation affects electronic coupling by changing the extent of orbital overlap between the donor (acceptor) and the bridge moiety, which seems quite obvious on the basis of quantum mechanics. Recent interest in cross-conjugated BLs for MV molecules is to verify the destructive quantum interference in charge transport of single-molecule conductance, aiming at development of molecular electronics [73, 74]. In this context, the *meta* (**XII**) and *para* phenylene pair is the prototype, which appears repeatedly in textbook to address phenomena like electronic resonance, π conjugation, and electron density distribution. The other example of cross-conjugated BL is σ-geminal-diethynylethene (**XIII**). **XII** and **XIII** have been used to link, for example, covalently bonded Mo_2 and Ru_2 units [75, 76] as well as organic triaryl groups [77] for constructing the MV systems. The decoupling effects of cross-conjugated BLs in the MV systems in solution are well established [75], in parallel with the results from the studies in terms of molecular conductivity.

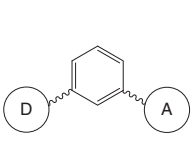

XIII

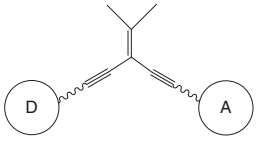

XII

Considering the relevance of ET to the biological systems, specifically DNA and proteins, hydrogen bond (HB) BLs were used to bridge donor and acceptor for MV D–B–A molecules [78]. In this regard, the HB-bridged MV systems are particularly of interest because the study can model ET induced by thermal fluctuations in the dark. The H-bond-bridged MV systems differ from those with covalent bond BLs in the molecular reflexibility and nuclear dynamics. Unfortunately, characteristic IVCT bands may not be observed in the HB-bridged systems [79, 80], being an obstacle for optical analysis. To strengthen the linkage between donor and acceptor, multiple

H-bonds are preferred [81, 82], but this seems not helpful in improving the visibility of the IVCT absorption. Study of HB D–B–A systems raise two fundamental issues, the efficiency of hydrogen bonds in transporting electrons and the coupling of electronic and nuclear degrees of freedom. Therefore, mechanistic aspect has been the focus of study in the area, specifically, how the bonded H atom(s) moves corresponding to electron transfer or vice versa. While the dominant theory is on the proton-coupled electron transfer (PCET), with respect to formation and cleavage of the bridging H-bond [83], a proton-uncoupled electron transfer (PUCT) is observed in H-bond mixed-valence system (**XIV**) recently [78]. Furthermore, in a MV D–B–A system, the bridging ligand may be functionalized so as to modulate the mixed valency in more than one state upon external stimulations such as light [84], pH, and redox reactions [85], which, therefore, are named as switching BLs. Typical examples of switching BLs are those incorporated with a dithenylethene group (**XV**) in order to make the extent of EC photo-switchable; as such, on/off status of electric conductance can be achieved by changing the radiation energy from ultraviolet to visible light [86].

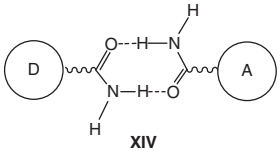

XIV

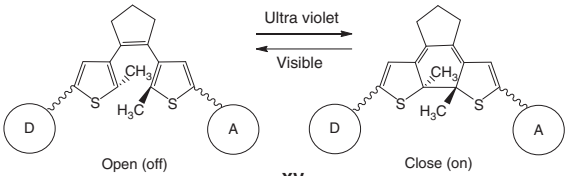

XV

1.4 Characterization and Evaluation of Mixed-Valence Systems

1.4.1 Electron Paramagnetic Resonance Spectroscopy

Mixed-valence compounds are paramagnetic with at least one unpaired electron. Thus, electron paramagnetic resonance (EPR) spectroscopy is a basic means for characterization of the electronic states and investigation of the mixed valency of the systems. For example, EPR spectroscopy is an important method used to elucidate the electronic and spin states of the Mn_4Ca cluster of the oxygen-evolving center (OEC) in photosynthesis II [87] and to characterize the mimic OEC complexes [88]. For some MV systems in which the hyperfine structures provide detailed information on the electron–nuclei coupling, EPR spectroscopy can be a powerful technique

for study of the D–A electronic interaction and the ET dynamics [55, 68, 89, 90]. Particularly, the EPR timescale of 10^{-6}–10^{-8} seconds, lower than the vibrational frequencies of solvent modes in sub-picoseconds, allows the relatively slow ET processes to be probed. For weakly coupled MV compounds, whose IVCT bands are not available, EPR spectra become an important technique that complements with the optical analysis [91]. Furthermore, using the EPR methods, temperature effect of thermal ET kinetics can be readily assessed by spectral simulations [56, 91, 92].

1.4.2 Electrochemical Methods

Electrochemical methods by measuring the chemical potentials of the redox centers are widely used for characterization of MV D–B–A compounds and for semiquantitative evaluation of the coupling strength. Separation of half-wave potentials between two successive one-electron oxidations (or reduction) occurring on each of the two redox centers, $\Delta E_{1/2}$, is recorded by cyclic voltammetry (CV) or differential pulse voltammetry (DPV) [93]. The magnitude of $\Delta E_{1/2}$ dictates the coupling extent between the D and A sites. For the members in a homologous series sharing a common donor and acceptor, the larger the $\Delta E_{1/2}$ value, the stronger the EC. A superficial explanation for this is that electronic coupling, through either electrostatic or electronic resonant effects, brings the positive charge from the site where electron is removed to the other site such that its oxidation potential increases, as a result, enlarging the $\Delta E_{1/2}$ value. In fact, there are more factors that affect the magnitude of $\Delta E_{1/2}$. From $\Delta E_{1/2}$, the free energy change (ΔG_c) and equilibrium constant K_C for comproportionation of the mixed-valence species can be determined (Eq. 1.3c–d) [8].

$$[\text{D–B–A}]^n + [\text{D–B–A}]^{(n+2)} \rightleftharpoons 2[\text{D–B–A}]^{(n+1)} \tag{1.3a}$$

or,

$$[\text{D–B–A}]^n + [\text{D–B–A}]^{(n-2)} \rightleftharpoons 2[\text{D–B–A}]^{(n-1)} \tag{1.3b}$$

$$\Delta G_C = -RT \ln K_C \tag{1.3c}$$

$$K_C = \exp(\Delta E_{1/2}/25.69) \tag{1.3d}$$

where $\Delta E_{1/2}$ is measured in millivolts (mV) at 25 °C. The magnitude of ΔG_C, which measures the thermodynamic stability of the MV species, is the sum of several energetic factors [8, 94]

$$\Delta G_c = \Delta G_e + \Delta G_r + \Delta G_i + \Delta G_s \tag{1.4}$$

Of the four terms that contribute to ΔG_c, ΔG_e (electrostatic effect) and ΔG_r (electronic resonance effect) jointly account for the strength of electronic interaction between the D and A sites. The other two terms, statistic ($\Delta G_s = 4$) and inductive factors (ΔG_i), are generally small and similar in value for homologous systems;

therefore, ΔG_c can be divided into the resonance and nonresonance two components [25], i.e.

$$\Delta G_c = \Delta G_r + \Delta G_{nr} \tag{1.5}$$

ΔG_{nr} includes all the nonresonance contributions to the overall free energy change, i.e. ΔG_e, ΔG_i, and ΔG_s. ΔG_r is dominated by orbital interactions between the donor and acceptor. The contributions of these two terms to the comproportionation equilibrium are expressed by the following reactions,

$$[D–B–A]^n + [D–B–A]^{(n+2)} \rightleftharpoons 2\{[D–B–A]^{(n+1)}\}_0 \qquad \Delta G_{nr} \tag{1.6a}$$

$$2\{[D–B–A]^{(n+1)}\}_0 \rightleftharpoons 2[D–B–A]^{(n+1)} \qquad \Delta G_r \tag{1.6b}$$

In Eq. (1.6), $\{[D–B–A]^{(n+1)}\}_0$ represents the zero-interaction (charge localized) MV compound, and the second reaction shows explicitly that ΔG_r is the stabilization energy of two moles of the Class II or III MV complex by the D–A electronic interaction (delocalization) [25]. However, it should be noted that for those with different donors and acceptors, the $\Delta E_{1/2}$ values are not correlated to the EC content. Furthermore, application of electrochemical method has a low potential limit. The minimum of $\Delta E_{1/2}$ is 36.5 mV, when the compropotionation constant (K_C) reaches the statistical factor of 4 [95, 96]. For instance, this limit is approached with increasing the bridge length and lowering the symmetry compatibility between the donor (acceptor) and the BL. Evaluation of EC for a MV system may be performed at two levels in terms of accuracy, electrochemical measurements of $\Delta E_{1/2}$ for assessment of the electronic interaction and optical analysis of H_{ab} to quantitatively determine the degree of EC from the Mulliken–Hush expression (Eq. 1.1).

1.4.3 Optical Analysis

The most striking optical phenomenon for mixed-valence molecules is the absorption arising from the charge transfer from the donor to the acceptor (IVCT). Compared to the electronic transitions, the IVCT absorbance features low transition energy (E_{IT}) (usually appearing in the near-infrared or lower region) and low molar extinction coefficient (ε_{IT}) and broadness characterized by the half-height bandwidth ($\Delta\nu_{1/2}$); an asymmetric spectral profile is commonly found for moderately to strongly coupled MV systems. Analysis of IVCT absorption based on the Hush model (Eq. 1.1) gives rise to important chemical physical parameters in regard of D–A EC and ET. However, for Class I, the IVCT energy is high and the absorption is fairly weak, which may not be detectable spectroscopically. The basic relationship of energy conservation for the ET reaction in MV systems is given by [5, 17]

$$E_{IT} = \lambda + \Delta G^0 \tag{1.7}$$

where λ and ΔG^0 is the total reorganization energy and free energy change for the ET reaction, respectively. For symmetrical MV systems consisting of two electronically

identical redox centers, $\Delta G^0 = 0$, and thus, $E_{IT} = \lambda$, which gives the thermal activation energy equaling one quarter of the transition energy (or reorganization energy), i.e. $\Delta G^* = \lambda/4$ (Eq. 1.2) [97, 98]. Based on the Mulliken formalism, Hush showed that the electronic coupling integral H_{ab} can be calculated from the IVCT spectral parameters [5]. The Mulliken–Hush expression (Eq. 1.1) is applicable for Class II compounds in a broad range of extent of EC and has been widely used in MV systems with various redox centers [6–8, 10, 20, 23, 40]. However, it should be noted that the effective ET distance, r_{ab} in Eq. 1.1, is usually shorter than the geometric distance between the redox centers due to orbital overlap between the D (A) and BL moieties [99]. Furthermore, for sufficiently strong coupling systems, the IVCT band is narrowed as the low-energy side of the absorption envelope is cutoff [9, 10, 53, 57]. Therefore, direct measurements of the r_{ab} from the molecular structure and of the $\Delta\nu_{1/2}$ from IVCT band would bring significant errors to estimation of H_{ab}. The effective r_{ab} is related to the dipole moment change induced by the intervalence transition, which can be probed experimentally through electroabsorption (Stark effect) [100, 101]. In case where this technique is not available, judicial determination of r_{ab} with chemical tuition might be helpful. For strongly coupled systems, simulation of a Gaussian-shaped full IVCT band is necessary to accurately measure $\Delta\nu_{1/2}$ for calculation of H_{ab} using the Mulliken–Hush expression (Eq. 1.1). For delocalized Class III systems, $H_{ab} = E_{IT}/2$ [17, 19]. With the classical two-state treatment, electronic coupling leading to electron delocalization lowers the adiabatic potential minima by H^2_{ab}/λ relative to those in the diabatic system [25]. In symmetrical Class II system, from the comproportionation equilibrium, we have

$$\begin{aligned} -\Delta G_r &= 2H^2_{ab}/\lambda \\ &= 2H^2_{ab}/E_{IT} \end{aligned} \tag{1.8}$$

Similarly, for symmetrical Class III compounds, the resonance stabilization energy is the difference between the energies of two moles of fully delocalized compound (H_{ab}) and of the noninteraction mixed valence ($\lambda/4$), that is,

$$\begin{aligned} -\Delta G_r &= 2(H_{ab} - \lambda/4) \\ &= E_{IT} - \lambda/2 \end{aligned} \tag{1.9}$$

For borderline Class III systems [25], or Class II–III and Class III systems characterized by $H_{ab} \approx \lambda/2$, $-\Delta G_r \to \lambda/2$, while for very strong coupled systems, Class III with $H_{ab} \gg \lambda/2$, $-\Delta G_r \to \lambda$. Therefore, the strongly and very strongly coupled systems can be distinguished by comparison of the magnitudes of $\Delta E_{1/2}$ and E_{IT}. For borderline Class III compounds, $\Delta E_{1/2} \approx E_{IT}/2$, and for fully delocalized systems, $\Delta E_{1/2} \approx E_{IT}$. Knowing that for strong coupling systems $\Delta G_c \approx \Delta G_r$, and thus, $-\Delta G_r = \Delta E_{1/2}$, then the reorganization energy can be estimated by $\lambda = 2(E_{IT} - \Delta E_{1/2})$. These energetical correlations that combine electrochemical and spectral data are very useful for characterization of strongly coupled MV compounds [102].

1.5 Important Issues in Mixed-Valence Chemistry

1.5.1 System Transition in Mixed Valency from Localized to Delocalized

Mixed valency is designated to determine the extent of mixing oxidation states of the spatially separated atoms of the same element or the degree of electronic coupling between the bridged redox centers. The Robin–Day's classification of MV compounds has been widely employed to characterize individual MV compounds and to map the full landscape of MV systems in terms of mixed valency. The Robin–Day's three classes of MV compounds are distinguished by the IVCT spectral features and can be schemed by physical parameters, vibrational timescale, and coupling integral and reorganization energies. Fully localized Class I compounds with $H_{ab} \leq 10\,cm^{-1}$ exhibit a high-energy IVCT band usually beyond the visible region [1]. The IVCT bands for Class II compounds ($2H_{ab} < \lambda$) may appear in visible, near-infrared region, even the infrared region, depending on the degree of EC and the nature of the system. With increasing electronic coupling, the IVCT transition energy decreases, the bandwidth becomes narrow attributed to the cutting-off phenomenon, and the band shape is more asymmetric. Within the two-state theoretic framework, the IVCT bands for the borderline Class III compounds ($2H_{ab} \approx \lambda$) are expected to be sharp [9, 10, 57]. For the very strongly coupled compounds with $2H_{ab} \gg \lambda$, the valence electrons of the redox centers are fully delocalized so that an averaged oxidation state should be assigned to each of them. The charge transfer transition (IVCT) is transformed into electronic resonance between delocalized molecular orbitals where the valence electrons reside. In this case, the Robin–Day's classification is no longer applicable [1]; the "IVCT" band, as so called, is high in energy and more symmetric, showing the transition from vibronic to electronic [103]. From the distinct electronic structure, optical behavior, and energetic correlations for this category of MV compounds, *genuine delocalized systems* or Class IV are suggested in the literature [40, 102–104].

However, the Mulliken–Hush formalism is incapable of predicting the cutoff phenomenon of IVCT absorption and earlier work did not elucidate the band asymmetry of Class II compounds, which is the most important, observable feature for moderately strongly coupled systems. More specifically, how to understand the pronounced variations of band shape and intensity as intervalence system approaches the Class II–III borderline, and how to optically characterize the transition from localized to delocalized system are the key issues in MV chemistry, which have attracted significant attention in both experimental and theoretical studies for the recent decades [9, 10, 39, 40, 55, 57]. Both metal complex and organic intervalence compounds have been exploited to resolve these problems [39, 53, 105]. Experimental approaches to this issue is to create homologous series of MV compounds, (i) having different charge-bearing units but the same BL [39, 40] (ii) sharing the same redox sites linked with different ligands [53, 106], and (iii) alternation of the auxiliary ligands and coordinating atoms [66, 105], so that the optical parameters are mapped with increasing EC. Examples in the $d^{5\text{-}6}$ dinuclear metal complexes,

such as $[(bpy)_2ClRu(pz)RuCl(bpy)_2]^{3+}$ and $[(bpy)_2ClOs(pz)OsCl(bpy)_2]^{3+}$, $[(NH_3)_5Ru(pz)Ru(NH_3)_5]^{5+}$ $[(NH_3)_5Ru(4,4'\text{-bpy})Ru(NH_3)_5]^{5+}$, and $[(NH_3)_5Os(NN)Os(NH_3)5]^{5+}$, $[(NH_3)_5Ru(pz)Ru(NH_3)_5]^{5+}$, and $[(bpy)_2ClRu(pz)RuCl(bpy)_2]^{3+}$, show that with similar molecular structures, changes in metal and ligands can significantly alter the extent of electronic delocalization of the odd electron, leading to transition of the system from one MV regime to another [39]. In M_2–BL–M_2 (M = Mo and W) complex systems, it is reported that transition of mixed valency can be realized by changing the nuclearity of the dimetal units [104] or by alternation of the chelating atoms of BL [105, 107], while the molecular structures remain similar.

With intense investigations in various MV systems, the IVCT cutoff phenomenon is well understood in the two-state model framework. For strongly coupled symmetrical MV systems ($\Delta G^0 = 0$), the vibrational levels are unevenly populated in the vicinity of the equilibrium configuration of the reactant on the lower adiabatic surface because of the low activation energy (ΔG^*). This non-Boltzmann distribution of the vibrational states of the reactant ground state eliminates the spectral lines of Frank–Condon transition in low energy, consequently truncating the Gaussian-shaped band profile on the low-energy side of the IVCT band [24, 52, 57]. Therefore, for moderately strongly coupled Class II systems, an asymmetric IVCT band is observed with the bandwidth significantly narrower than the Gaussian-shaped spectrum with a half-height bandwidth $\Delta\nu_{1/2}$ (HTL) at the high-temperature limit (HTL) given by Eq. (1.10) [9, 10, 40, 57].

$$\Delta\nu_{1/2}(\text{HTL}) = \sqrt{16 \ln 2 k_B T \nu_{\max}} \tag{1.10}$$

The IVCT band gets more asymmetric as the coupling integral H_{ab} increases. Ideally, for systems on the Class II–III borderline, the IVCT band features the lowest transition energy ($E_{IT} = 2H_{ab}$) and a half-cut absorption at $2H_{ab}$ [9, 10, 105]. This unique optical feature leads to a proposal that defines a new class of mixed valency, namely, Class II–III [9, 39, 40, 53, 108].

1.5.2 Solvent Control of Electron Transfer

The three Robin–Day classes of MV compounds differ in the magnitude of H_{ab} and the ET rate (k_{et}) [109]. While Class I and III are considered to be fully electron localized and electron delocalized, respectively, electron transfer in Class II compounds can be very slow ($<10^{-6}$ seconds) or picosecond fast (10^{-12} seconds). Solvent molecules respond to change of charge density on the donor and acceptor by reorienting their electric dipoles. Here, the key issue is the timescale of electron migration relative to that of solvent molecule motions (stretching, rotational, and translational), which governs the ET dynamics [24]. Orientational energy of solvent molecules is in the range of 30–100 cm^{-1}; the vibrational transmission frequency ν_n is taken as $5 \times 10^{12}\ s^{-1}$ on average [6]. In Class II systems, when the ET scale is substantially smaller than ν_n, solvent molecules can quickly reorient their dipoles corresponding to the charge redistribution of the solute molecule, being the case where both electron and solvent are localized and ET proceeds nonadiabatically. Solvents differing in dipole polarity are characterized by static dielectric constant (ε_s). Polar solvents exert strong electrostatic interactions on the

charged solute molecules, which increases the outer-sphere (solvent) reorganization energy. Solvent effects on EC and ET in Class II MV regime are predicted by the Marcus dielectric solvation continuum theory [6, 8, 14, 15, 38]. In Class III, electron exchange between the donor and acceptor occurs at a frequency close to nuclear vibrational transmission. Variation of charge density on the two charge-bearing units is "invisible" to the solvent molecules. Solvent dipoles surrounding a discrete MV molecule are randomly arranged, being the case of electron delocalized and solvent averaged [24]. A complicated situation is encountered when the system approaches Class III or on the borderline Class II–III, where ET dynamics are in the timescale of picoseconds ($10^{12}\ s^{-1}$). In Class II–III, while electron exchange proceeds rapidly, solvent molecules, with slightly slower timescale, are unable to respond promptly. In this case, the MV system remains electron localized, but the solvent effect is averaged [110]. The distinct optical behaviors and solvation properties for the borderline species give the reasons that a new mixed-valency regime, Class II–III, is defined [9, 40]. After examining the electronic dynamics of a series of Ru_3–Ru_3 compounds in various solvents and under variable temperatures, Kubiak and coworkers found that solvent dynamic properties (relaxation time τ), rather than the dielectric property of solvent, exert a particular impact on electronic dynamics of the Class II–III borderline systems [108]. The study points out that in Class II–III system, ET is controlled by time-dependent parameters (i.e. solvent relaxation times and moments of inertia) of solvents, but not by the static parameters of solvents.

1.6 Theoretical Background

1.6.1 Potential Energy Surfaces from Classical Two-State Model

The semiclassical two-state model was first used as a theoretical model to elucidate chemical transformation between particles (atoms, ions, and colloids) in earlier 1930s by Landau & Zener [111, 112]. It was adopted to illustrate the kinetics and energetics of electron transfer by Kubo and Toyozawa [11], Marcus [14, 15], Levich & Doganadze [12, 13, 41], and by Hush to derive the calculation equation of coupling constant H_{ab} from intervalence parameters in MV systems [5]. The two-state model can be interpreted in classical and quantum mechanics ways. The overall energy for a solvated molecule is contributed by electron and nuclei in motion, and the interactions between them. It changes as the electronic and nuclear configurations of the system (molecule + surrounding solvent molecules) change. Typically, in a mixed-valence system, removal of an electron from the donor and simultaneously addition of an electron to the acceptor induce variations of the nuclear configurations, and back and forth movements of the odd electron between the donor and acceptor result in energy fluctuation of the system. In the classical Marcus theory [113], the reactant and product potential energies are modeled by a harmonic oscillator. On this potential curve, the ordinate represents the potential

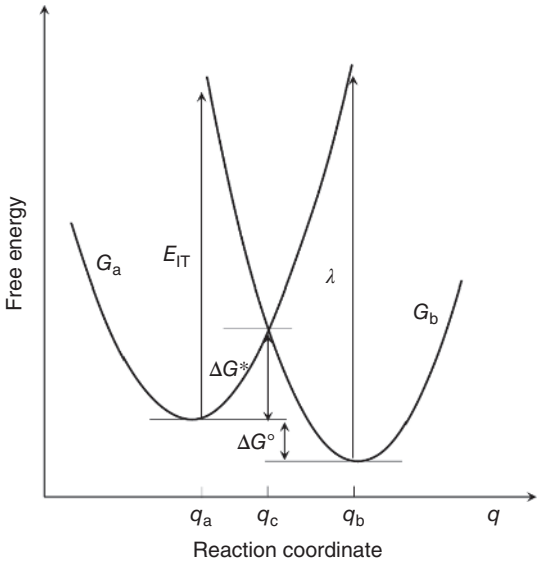

Figure 1.3 Diabatic free energy surfaces of the reactant (G_R) and the product (G_P) against the reaction coordinate for the ET reaction in asymmetric MV D–B–A system with $E_{IT} = \lambda + \Delta G^\circ$ and $\Delta G^* = \lambda/4$.

energy that becomes free energy with ignoring entropy changes (ΔS), and the abscissa measures the change of nuclear configuration or nuclear coordinate q. The potential energy of this oscillator, G_a for the reactant and G_b for the product, varies as a function of deviation ($q-q_c$) from nuclear equilibrium position (q_c) caused by electron transfer, which is then described pictorially by a parabolic curve and mathematically by a quadratic equation.

$$G = 1/2f(q_0 - q)^2 \tag{1.11}$$

where f is the oscillator strength or force constant. The diabatic potential energy surfaces for electron transfer system is constructed by the reactant (G_a) and product (G_b) potential curves crossing each other at the equal nuclear configuration q^*, as shown in Figure 1.3.

$$G_a = 1/2f(q_a - q)^2 \tag{1.12a}$$

$$G_b = 1/2f(q - q_b)^2 \tag{1.12b}$$

$$\lambda = 1/2f(q_a - q_b)^2 \tag{1.13}$$

Eq. (1.13) was used by Marcus [113, 114] and Hush [17] to define the reorganization energy for electron transfer. When the separation of the minima of the noninteracting reactant and product parabolas, ($q_a - q_b$) is replaced by a_0, and the displacement along the reaction coordinate by x, the reaction process is scaled by a dimensionless coordinate X ($=x/a_0$). X varies from 0 ($x = 0$) to 1 ($x = 1$) as the reaction proceeds from reactant to product [7]. Then, G_a and G_b are given with respect to X (Eq. (1.14a) and (1.14b)).

$$G_a = fx^2/2 = \lambda X^2 \tag{1.14a}$$

$$G_b = f(x - a_0)^2/2 + \Delta G^0 = \lambda(X-1)^2 + \Delta G^0 \tag{1.14b}$$

$$(G_b - G_a) = (\lambda + \Delta G^0) - 2\lambda X \tag{1.14c}$$

or,

$$X^2 = [\lambda + \Delta G^0 - (G_b - G_a)]^2/4\lambda^2 \tag{1.14d}$$

where ΔG^0 is the change of free energy for the electron transfer reaction. G_a and G_b cross at the transition state X^*, where $E^*_R = E^*_P$ and $X^* = (\lambda + \Delta G^0)/2\lambda$. Substituting X^* to Eq. (1.14a) and (1.14b), we obtain the free energy barrier for asymmetric electron transfer, ΔG^* ($= G^*_a = G^*_b$) [11, 17, 38, 97, 98],

$$\Delta G^* = (\lambda + \Delta G^0)^2/4\lambda \tag{1.15}$$

For symmetric mixed-valence systems, $\Delta G^0 = 0$, and then, $\Delta G^* = \lambda/4$. In the Marcus theory, this is the energy barrier for thermal electron transfer at the nonadiabatic limit [14, 15]. In an exothermal electron transfer reaction, $\Delta G^0 < 0$, which is the case described by Figure 1.3, while an endothermic reaction has $\Delta G^0 > 0$. The reaction driving force is conventionally designated by $-\Delta G^0$. The quadratic nature of Eq. (1.15) gives rise to three scenarios, known as the Marcus defined three regions [7, 115], as shown schematically in Figure 1.4. In the different region, the ΔG^* and thus the ET rate (k_{et}) correlate with the magnitude of ΔG^0 relative to λ in different ways. In the normal region, where $-\Delta G^0 < \lambda$, increasing the driving force lowers the energy barrier, and as a result, ET is speeded up. Further increasing the driving force to $-\Delta G^0 = \lambda$, the system enters the barrierless region ($\Delta G^* = 0$). When $-\Delta G^0 > \lambda$, from Eq. (1.15), large driving leads to increase of the energy barrier and reduction of the ET rate, which is called the inverted region.

1.6.2 Quantum Description of the Potential Energy Surfaces

Alternatively, the diabatic potential surfaces for electron transfer process can be built by quantum mechanics from the diabatic initial (ϕ_I) and final (ϕ_F) electronic states, in which the transferring electron resides on the donor and acceptor, respectively [19]. Suitable electronic wave functions that define the diabatic states can be obtained by interpreting results obtained by making electronic structure calculations within the Born–Oppenheimer framework, that is

$$\psi(r, Q) = \phi(r, Q)\chi(Q) \tag{1.16}$$

The implication of using the reduced wave functions $\phi(r, Q)$ is that the electronic wave functions for the electron in motion are instantaneously adjusted to change of the nuclear coordinate (Q) caused by nuclear dynamics, such as molecular vibrations, bond break and form. Diabatic wave functions can be constructed as sums of wave functions of that form so as to allow the transferring charge to become exposed for study. Each diabatic state has an associated potential energy varying as a function of Q due to nuclear motion,

$$E(Q) \equiv \langle \phi_I(Q) \mid \boldsymbol{H} \mid \phi_F(Q) \rangle \tag{1.17}$$

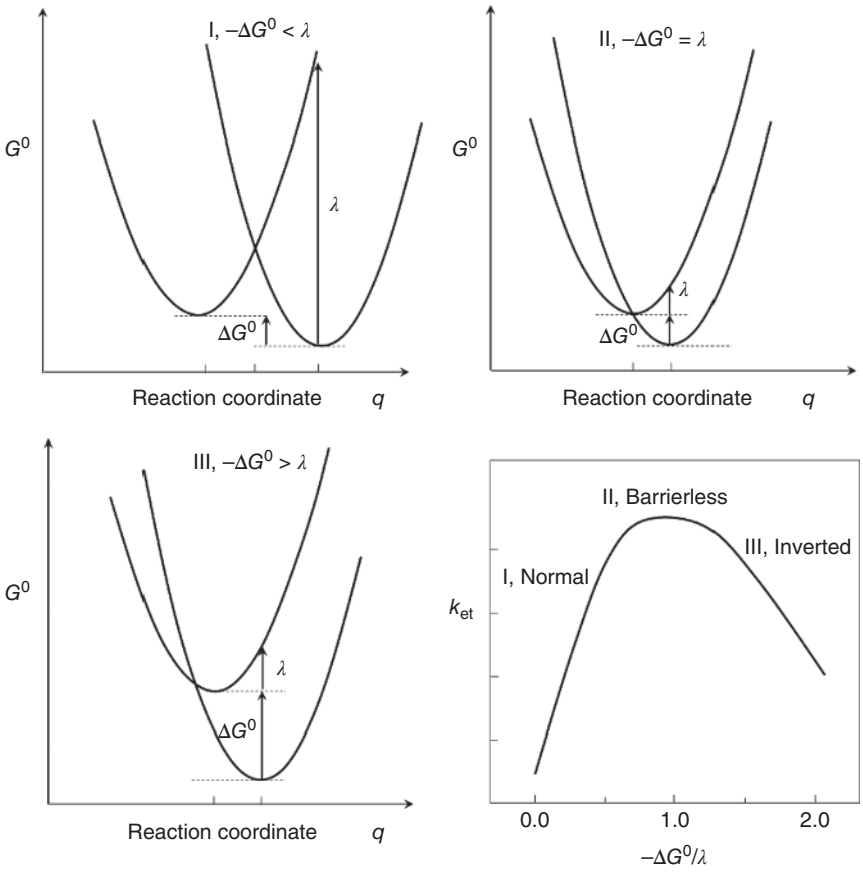

Figure 1.4 Plot of the free energy (G^0) versus the reaction coordinate q for three different values of ΔG^0 that corresponds to the three regions of Marcus, I, II, and III, respectively.

where $\boldsymbol{H}$ is the electronic Hamiltonian with Q dependence for the initial and final diabatic states [19].

Interaction of initial diabatic state with the final one with respect to the zeroth-order electronic Hamiltonian $\boldsymbol{H}$ of the system gives rise to the diabatic representation of potential energy profiles for electron transfer along the reaction coordinate Q that connects the minima of the reactant (G_a) and product (G_b) wells.

$$H_{aa} = \langle \phi_a \mid \boldsymbol{H} \mid \phi_a \rangle = G_a \tag{1.18a}$$

$$H_{bb} = \langle \phi_b \mid \boldsymbol{H} \mid \phi_b \rangle = G_b \tag{1.18b}$$

The eigenvalues (G_a) and (G_b) cross at the intersection Q^* that defines the diabatic activation energy ΔG^* for thermal electron transfer for Class I, in accordance with the classical description (Figure 1.3). The interaction between the reactant and product states produces the electron transfer integral H_{ab}

$$H_{ab} = \langle \phi_a \mid \boldsymbol{H} \mid \phi_b \rangle \tag{1.19}$$

Linear combination of the two diabatic states ϕ_a and ϕ_b generates the adiabatic ground (lower) ψ_g and excited (upper) ψ_e states [9, 97],

$$\psi_g = c_a\phi_a + c_b\phi_b \tag{1.20a}$$

$$\psi_e = c_a\phi_a - c_b\phi_b \tag{1.20b}$$

The mixing coefficients are normalized, i.e.

$$c_a^2 + c_b^2 = 1 \tag{1.20c}$$

where $c_a{}^2$ and $c_b{}^2$ are the fraction of the transferring charge on the donor and acceptor, respectively, at any given nuclear configuration. The energies of the adiabatic states, G_g and G_e, and the interaction integral H_{ab} can be obtained by solving the two-state secular determinant:

$$\begin{vmatrix} H_{aa} - G & H_{ab} \\ H_{ab} & H_{bb} - G \end{vmatrix} = 0 \tag{1.21}$$

where $H_{aa} = G_a$ and $H_{bb} = G_b$, if the overlap integral S_{ab} is neglected. The electronic coupling between the two diabatic states leads to the formation of two new surfaces, the first-order or adiabatic states of the system [7].

$$G_g = 1/2\left\{(G_a + G_b) - \left[(G_b - G_a)^2 + 4H_{ab}^2\right]^{1/2}\right\} \tag{1.22a}$$

$$G_g = 1/2\left\{(G_a + G_b) + \left[(G_b - G_a)^2 + 4H_{ab}^2\right]^{1/2}\right\} \tag{1.22b}$$

The adiabatic potential surfaces are constructed along with the reaction coordinate X.

$$G_g = \frac{[\lambda(2X^2 - 2X + 1) + \Delta G^0]}{2} - \frac{\left[(\lambda(1 - 2X) + \Delta G^0)^2 + 4H_{ab}^2\right]^{1/2}}{2} \tag{1.23a}$$

$$G_e = \frac{[\lambda(2X^2 - 2X + 1) + \Delta G^\circ]}{2} + \frac{\left[(\lambda(1 - 2X) + \Delta G^\circ)^2 + 4H_{ab}^2\right]^{1/2}}{2} \tag{1.23b}$$

With G_g and G_e determined, the coefficients c_a and c_b can be obtained by solving the equations [116]

$$\begin{pmatrix} H_{aa} - G_g & H_{ab} \\ H_{ab} & H_{bb} - G_g \end{pmatrix}\begin{pmatrix} c_a \\ c_b \end{pmatrix} = 0$$

$$\begin{pmatrix} H_{aa} - G_e & H_{ab} \\ H_{ab} & H_{bb} - G_e \end{pmatrix}\begin{pmatrix} -c_b \\ c_a \end{pmatrix} = 0$$

Then, the product of the mixing coefficients is given by Eq. (1.24).

$$c_a c_b = H_{ab}/(G_e - G_g) = H_{ab}/E_{IT} \tag{1.24a}$$

$$c_a c_b = \frac{1}{2}\left[1 - \left(\frac{G_b - G_a}{G_e - G_g}\right)^2\right]^{1/2} \tag{1.24b}$$

Figure 1.5 plots the variations of the diabatic and adiabatic free energies along the reaction coordinate and the correlations between them.

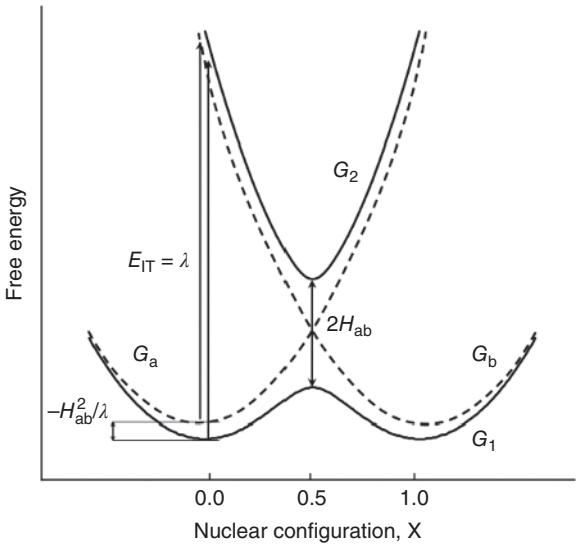

Figure 1.5 Plots of the diabatic (dashed line) and adiabatic free energy curves for ET reaction in a symmetric MV D–B–A system ($\Delta G° = 0$).

Equation (1.23) dictates that for a symmetric system, there are two energy minima ($G_g = G_e = 0$) at $X = 0$ and $X = 1$, if $H_{ab} = 0$, which is the diabatic representation. As a result of electronic coupling, H_{ab} increases, the minima for the adiabatic ground state (G_g) is lowered in energy by $H^2{}_{ab}/\lambda$, and shifted toward the half way ($X^* = 0.5$), getting close to each other, as shown in Figure 1.5. Then, the adiabatic minima are located at

$$\frac{1}{2}\left\{1 - \left[1 - 4(H_{ab}/\lambda)^2\right]^{1/2}\right., \quad \frac{1}{2}\left\{1 + \left[1 - 4(H_{ab}/\lambda)^2\right]^{1/2} \right. \tag{1.25}$$

compared to 0 and 1, respectively, for the diabatic surfaces [9].

The difference between the adiabatic energies is given by

$$\begin{aligned}(G_e - G_g) &= \left[(G_b - G_a)^2 + 4H_{ab}^2\right]^{1/2} \\ &= \left\{[\lambda(1 - 2X + \Delta G^0)^2 + 4H_{D,A}^2\right\}^{1/2} \qquad (1.26a)\\ (G_e + G_g) &= (G_b + G_a)^2 \\ &= \lambda(2X^2 - 2X + 1) + \Delta G^0 \qquad (1.26b)\end{aligned}$$

Equation (1.26a) shows that the intervalence transition maximum occurs at the reactant minimum ($X = 0$) with $E_{IT} = \lambda$ if $H_{ab} = 0$ and that the adiabatic states are separated at $X = 0.5$ by $2H_{ab}$ (Figure 1.5). In a symmetric adiabatic system, the vertical transition at the equilibrium configuration of the reactants (or products) remains equal to λ regardless of the magnitude of the electronic coupling as long as the system remains valence trapped.

The reaction coordinate X is related to c_b^2, which equals the charge transferred to the acceptor from the donor by

$$c_b^2 = \frac{1}{2}\left[1 - \frac{(1 - 2X)}{\{[(1 - 2X) + \Delta G/\lambda]^2 + 4H_{ab}/\lambda^2\}^{1/2}}\right] \tag{1.27}$$

Both X and ${c_b}^2$ measure the progress of the electron transfer by nuclear coordinate and electronic coordinate, respectively. From Eq. (1.27), the two coordinates are not linearly related until $H_{ab}/\lambda \geq 1$. Also, in the diabatic limit ($H_{ab} = 0$), there is no electron density transferred until $X = 0.5$ at which the electron "suddenly" jumps over the intersection [19]. In this case, ${c_b}^2$ is not a continuous function of X: instead ${c_b}^2 = 0$ for all $X < 1/2$ and ${c_b}^2 = 1$ for $X > 1/2$. As H_{ab} increases, the charge fraction transferred to the acceptor increases gradually with variation of nuclear coordinate from $X = 0$ to $X = 1$. At the transition state ($X = 1/2$), ${c_b}^2$ always equals 1/2. It is easy to prove that for symmetrical system with $2H_{ab} < \lambda$ (Class II), the transferred charge fraction at the equilibrium is given by

$$\left(c_b^2\right)_{eq} = \frac{1}{2}\left[1 - \left(1 - \frac{4H_{ab}^2}{\lambda^2}\right)^{1/2}\right] \tag{1.28}$$

For a borderline Class III system ($2H_{ab} = \lambda$), ${c_b}^2 = 1/2$, indicating electron delocalization.

For the symmetric MV systems ($\Delta G^0 = 0$) [25], the free energy of activation for the adiabatic ET reaction (thermal exchange) is given by Eq. (1.19)

$$\begin{aligned} \Delta G^* &= \lambda/4 - H_{ab} + H_{ab}^2/\lambda \\ &= (\lambda - 2H_{ab})^2/4\lambda \end{aligned} \tag{1.29}$$

Equation (1.29) shows that adiabatic ΔG^* is a sum of three terms. The first term is the ΔG^* in nonadiabatic limit, the second term is from the coupling integral that contributes to lower the activation energy by half-splitting of the upper and lower surfaces, and the last term, ${H_{ab}}^2/\lambda$, increases the reaction barrier through stabilization of the reactant (Figure 1.5). Equation (1.29) holds for a broad range of Class II compounds for which the self-exchange reaction is described by a double-well potential, that is, from weakly coupled Class II to the borderline of Class II–III. When further increasing the donor–acceptor coupling to $2H_{ab} > \lambda$, the lower energy surface features a single well at $X = 1/2$. This is the case of electron delocalization ($\Delta G^* = 0$), Class III. For the asymmetrical adiabatic system ($\Delta G^0 \neq 0$), the free energy of activation is given by Eq. (1.30) [25],

$$\Delta G^* = \frac{\lambda}{4} + \frac{\Delta G^0}{2} + \frac{(\Delta G^0)^2}{4(\lambda - 2H_{ab})} - H_{ab} + \frac{(H_{ab})^2}{4(\lambda + \Delta G^0)} \tag{1.30}$$

1.6.3 Reorganization Energies

Equation (1.7) is the basic and important energetic relationship for electron transfer reaction in MV chemistry. This equation, $E_{IT} = \lambda + \Delta G^0$, dictates that the absorbed photon energy (E_{IT}) is used to rearrange the nuclear configuration for ET (λ) and to change the free energy of the sysytem (ΔG^0). For an endothermic reaction, $\Delta G^0 > 0$, and for an exothermic reaction, $\Delta G^0 < 0$. The reorganization energy is to overcome the Frank–Condon barrier of intervalence transition. This portion of energy is dispatched through radiationless relaxation after the electron transfer process and does not contribute to free energy of the system. For ET in condensed medium, the total

reorganization energy (λ) was divided into two portions [15, 38]. One portion is for adjustment of the intramolecular nuclear configuration, namely, inner reorganization energy, (λ_{in}), and the other is to control the intermolecular nuclear configuration, (λ_{out}) [7, 14, 17, 97, 98].

$$\lambda = \lambda_{in} + \lambda_{out} \tag{1.31}$$

λ_{in} and λ_{out} are dominated by the high-frequency vibration modes (>1000 cm^{-1}) of the molecule and the low-frequency vibrational modes (<100 cm^{-1}) of solvent molecules, respectively, therefore, being termed sometimes as λ_v and λ_s, respectively. Although λ_{in} and λ_{out} are conceptually well defined, practically, splitting of the total reorganization remains challenging. For most of mixed-valence systems, there are many vibrational modes contributing to the inner reorganization energy; it is difficult to identify the dominant models and determine their frequencies. In the 1950s, Marcus developed the dielectric continuum theory (Eq. 1.32), which originally was for out-sphere electron transfer reaction in solution [14, 15] that is applicable to determine the quantity of outer reorganization energy in the MV systems [6, 7, 25, 98].

$$\lambda_{out} = (\Delta e)^2 \left\{ \frac{1}{2a_1} + \frac{1}{2a_2} - \frac{1}{R} \right\} \left\{ \frac{1}{\varepsilon_\infty} - \frac{1}{\varepsilon_0} \right\} \tag{1.32}$$

With contribution of inner vibrations proposed originally by Hush, the Marcus–Hush theory was framed for electron transfer in the adiabatic limit [97, 98]. Without approximation, Eq. (1.32) was derived by Li using nonequilibrium statistical mechanics recently [117, 118]. Using the dielectric continuum model to treat a MV D–B–A system, both the donor and acceptor are viewed as a rigid sphere with radii a_1 and a_2, separated by R, and the molecule as a whole is bathed in solvent molecules with dielectric continuum. In Eq. (1.33), ε_∞ and ε_c are the optical and static dielectric constants of the medium, respectively, and Δe is the amount of charge transferred. For systems in which the electronic coupling is significant, electron delocalization causes the transferred charge be less than a unit. In this case, we can calculate the "real" charge transferred from the mixing coefficients (c_a and c_b) of the diabatic states. As a consequence of electron delocalization, the charge reduced at the equilibrium configuration of the donor is

$$\Delta q = \left(c_a^2 - c_b^2\right)_{eq} = \left(1 - 2c_b^2\right)_{eq} \tag{1.33}$$

From Eq. (1.28),

$$\left[\left(1 - c_b^2\right)_{eq}\right]^2 = \left(1 - \frac{4H_{ab}^2}{\lambda^2}\right) \tag{1.34}$$

Thus, the "real" charge-transferred Δe is $e\Delta q$, where e is the charge of one single electron. Accordingly, the solvent reorganization λ_{out} in Eq. (1.32) should be scaled by $(1 - 4H^2{}_{ab}/\lambda^2)$, giving

$$\lambda'_{out} = \lambda_{out}\left(1 - 4H_{ab}^2/\lambda^2\right) \tag{1.35a}$$

Similarly,

$$\lambda'_{in} = \lambda_{in}\left(1 - 4H_{ab}^2/\lambda^2\right) \tag{1.35b}$$

Consequently,

$$\lambda' = \lambda'_{in} + \lambda'_{out} = \lambda\left(1 - 4H_{ab}^2/\lambda^2\right) \tag{1.36a}$$

or,

$$\lambda = \lambda' + 4H_{ab}^2/\lambda \tag{1.36b}$$

Equations (1.35) and (1.36) show that partial electron delocalization lowers the reorganization energy to λ' but stabilizes the ground state and destabilizes the excited state, which increases the reorganization by $4H_{ab}^2/\lambda$. For Class II systems, these two effects cancel each other so that the optical transition energy (E_{IT}) remains equal to λ regardless of the degree of localization.

1.6.4 Electronic Coupling Matrix Element and the Transition Moments

In the previous section, we have defined the electronic matrix element H_{ab} that controls the thermal electron transfer between the donor and acceptor through electronic interactions between the diabetic reactant and product states (Eq. 1.19). In a similar vein, the intensity of optical electron transfer at the adiabatic equilibrium of the reactant is governed by the transition dipole moment, μ_{ge}.

$$\mu_{ge} \equiv \langle \psi_g \mid \boldsymbol{\mu} \mid \psi_e \rangle \tag{1.37a}$$

where $\boldsymbol{\mu}$ is the electronic dipole operator. ψ_g and ψ_g are the linear combinations of the diabatic states ϕ_a and ϕ_b with a mixing coefficient c_a and c_b (Eq. 1.20), respectively. Substitution for ψ_g and ψ_e from Eqs. 1.20a and 1.20b gives

$$\mu_{ge} = c_a c_b(\mu_b - \mu_a) \tag{1.37b}$$

From $c_a c_b = H_{ab}/E_{IT}$ (Eq. 1.24a), it follows that

$$\frac{H_{ab}}{E_{IT}} = \left|\frac{\mu_{ge}}{\mu_b - \mu_a}\right| \tag{1.38}$$

Defining the effective electron transfer distance $r_{ab} \equiv |(\mu_b - \mu_a)|/e$, the coupling integral H_{ab} is related to transition dipole moment μ_{ge} by

$$H_{ab} = \frac{E_{IT}|\mu_{ge}|}{e r_{ab}} \tag{1.39}$$

Expression of Eq. (1.39) may be considered to be a generalization of the Marcus–Hush theory (GMH) [119]. Hush showed that μ_{ge} is related to oscillator strength f and energy of the transition by [3]

$$|\mu_{ge}|^2 = f/1.085 \times 10^{-5} E_{IT} \tag{1.40a}$$

Assuming a Gaussian IVCT band for the weakly coupled Class II systems,

$$f = 4.6 \times 10^{-9} \varepsilon_{IT} \Delta\upsilon_{1/2} \tag{1.40b}$$

Combining and rearranging these equations gives the square of H_{ab}

$$(H_{ab})^2 = \frac{4.24 \times 10^{-4} E_{IT} \varepsilon_{IT} \Delta\upsilon_{1/2}}{(r_{ab})^2} \tag{1.41}$$

which is exactly the same as Eq. (1.1), known as the Mulliken–Hush expression.

By definition, the effective ET distance r_{ab} is determined by the dipole displacement of the diabatic states when a unit of charge (e) is transferred from the donor to the acceptor. r_{ab} is usually much less than r_0, the distance separating the localized charge centroids of the donor and acceptor because of electron delocalization. The diabatic dipole moment difference, $(\mu_b - \mu_a)$ is related to the ground dipole moment change $\Delta\mu$ upon electron transfer and the transition dipole moment μ_{ge} by

$$(\mu_b - \mu_a) = \left[\Delta\mu^2 + 4(\mu_{ge})^2\right]^{1/2} \tag{1.42a}$$

Measurements of $\Delta\mu$ and μ_{ge} can be achieved by electroabsorption (second-order Stark) spectroscopy, which probes the extent of charge redistribution with the charge transfer transition [101, 120]. Combining Eqs. (1.42a) with (1.39) gives

$$\Delta\mu^2 = (\mu_b - \mu_a)^2 \left[1 - 4(H_{ab}/E_{IT})^2\right] \tag{1.42b}$$

According to Eq. (1.39) and Eq. (1.42b), for a Class III system ($E_{IT} = 2H_{ab}$), $\Delta\mu = 0$, and $\mu_{ge} = (\mu_b - \mu_a)/2$, while for Class II,

$$\Delta\mu = (\mu_b - \mu_a)\left[1 - 4(H_{ab}/E_{IT})^2\right]^{1/2} \tag{1.42c}$$

Equation (1.42c) shows the dependence of $\Delta\mu/(\mu_b - \mu_a)$ on H_{ab} for symmetrical systems. For a Class II system, μ_{ge} varies as a function of H_{ab}; contrarily, for a Class III system ($2H_{ab} > \lambda$), μ_{ge} is independent of H_{ab}.

1.6.5 The Generalized Mulliken–Hush Theory (GMH)

Equation (1.39) shows that the diabatic coupling integral H_{ab} and the difference of the diabatic dipole moments ($\Delta\mu_{ab} \equiv \mu_b - \mu_a$) are correlated to the adiabatic transition dipole moment (μ_{ge}) and transition energy (E_{IT}). This transformation is implemented based on the assumption that transition moments connecting the diabatic states localized on different sites are zero ($\mu_{ab} = 0$). This transformation, which allows diabatic states to be defined in terms of purely adiabatic quantities, has general significance. As shown above, in the two-state limit, Eq. (1.39) turns to Eq. (1.1) or Eq. (1.42), the usual form of Mulliken–Hush expression. Eq. (1.39) actually provides a general method for determination of the off-diagonal matrix element from either experimental or theoretical data for the corresponding adiabatic systems, therefore, denoted as the generalized Mulliken–Hush (GMH) model. The GMH method is applicable for both symmetric and asymmetric mixed valence systems involving multiple electronic states and for various electron transfer processes (thermal, optical, and photoinduced) [121]. In application of the GMH model (Eq. 1.39) for Class II systems with a Gaussian IVCT band, the transition dipole moment μ_{ge} can be calculated from spectral parameters by

$$\mu_{ge} = 2.06 \times 10^{-2}(\varepsilon_{IT}\Delta\upsilon_{1/2}/E_{IT})^{1/2} \tag{1.43}$$

For mixed-valence systems presenting an asymmetrical IVCT band, the transition dipole moment is generally calculated from the integrated band area by [24, 116]

$$|\mu_{ge}|^2 = \frac{3hc\varepsilon_0 \ln 10}{2\pi^2 N_A} \int \frac{\varepsilon(\bar{\nu})}{\bar{\nu}} d\bar{\nu} \tag{1.44a}$$

$$|\mu_{ge}|^2 = 4.0 \times 10^{-4} \int \frac{\varepsilon(\bar{\nu})}{\bar{\nu}} d\bar{\nu} \tag{1.44b}$$

according to Eq. (1.44a) and (1.44b). With the μ_{ge} value, the difference of diabatic dipole moments $\Delta\mu_{ab}$ ($=\mu_b - \mu_a$) can be calculated from Eq. (1.42a) [119], in which the dipole moment change $\Delta\mu$ induced by electron transfer is determined by electrospectroscopy (Stark effect) [100, 101], or from quantum chemical calculations [99], or alternatively by estimation of the effective electron transfer distance ($\Delta\mu \equiv er_{ab}$) from the molecular geometry.

1.6.6 Analysis of IVCT Band Shape

In the high-temperature limit of classical treatment, the molar absorptivity of a charge transfer transition at a given transition energy ($h\nu$) is determined by the transition probability with Boltzmann distribution of the vibrational states over the energy surface of the ground-state configuration. Then, the absorption intensity $\varepsilon(\nu)$ relative to the maximum absorption ε_{max} at λ can be calculated from the energy difference relative to the equilibrium of the ground-state configuration from Eq. (1.45)

$$\varepsilon(\upsilon) = \varepsilon_{max} \exp[-(G_g - G_{g,eq})/RT] \tag{1.45a}$$

In considering the zeroth order interaction, $G_b = G_a$ and $G_a = \lambda X^2$ (Eq. 1.14a), and Eq. (1.45a) is converted into Eq. (1.45b).

$$\varepsilon(\upsilon) = \varepsilon_{max} \exp[-\lambda X^2/RT] \tag{1.45b}$$

Since $(G_2 - G_1) = h\nu$ and $\lambda + \Delta G^0 = h\nu_0$, X^2 in Eq. (1.14d) is expressed by

$$X^2 = [h\nu_0 - h\nu]^2/4\lambda^2 \tag{1.46}$$

Therefore,

$$\varepsilon(\upsilon) = \varepsilon_{max} \exp[-(h\nu_0 - h\nu)/4\lambda RT] \tag{1.47}$$

Equation (1.47) predicts a Gaussian-shaped band profile that can be obtained by plotting $\varepsilon(\nu)$ against $h\nu$, and the band maximum ε_{max} appears at $h\nu_0 = h\nu_{max} = \lambda + \Delta G^0$. The half-bandwidth (full band at half-height) $\Delta\nu_{1/2}$ measures the energy separation between $(h\nu_0 + h\nu)$ and $(h\nu_0 - h\nu)$, or $2h\nu$, at which $\varepsilon(\nu)/\varepsilon_{max} = 1/2$. Therefore, theoretical prediction of $\Delta\nu_{1/2}$ for the Gaussian-shaped band is given by Eq. (1.10) or

$$\Delta\upsilon_{1/2} = \Delta\,\upsilon_{high} + \Delta\,\upsilon_{low} = 2[4\ln(2)\lambda RT]^{1/2} \tag{1.48a}$$

where $\Delta\nu_{high} = \Delta\nu_{low} = [4\ln(2)\lambda RT]^{1/2}$ [9]. At room temperature, Eq. (1.49a) is reduced to

$$\Delta\upsilon_{1/2}{}^{II} = (2310\lambda)^{1/2} \tag{1.48b}$$

Equation (1.48) is applicable for weakly coupled Class II systems. As electronic coupling increases, the cutoff phenomenon occurs, resulting in asymmetric IVCT band with the low-energy side being truncated, and the measured $\Delta\nu_{1/2}$ will be significantly narrower than the calculated value. In fact, Class II defined by $2H_{ab} < \lambda$ covers a broad range of MV compounds from weakly to moderately

strongly coupled that shows significant asymmetry of the IVCT absorption. For those with $\lambda > 2H_{ab} < (\lambda - \Delta\nu_{1/2})$, the cutoff is small, and $\Delta\nu_{1/2}{}^{II}$ is determined by Eq. (1.48). But further increasing coupling until $\lambda > 2H_{ab} > (\lambda - \Delta\nu_{1/2})$, the cutoff reduces the low-energy side from $\Delta\nu_{lo}$ to $(\lambda - 2H_{ab})$, while $\Delta\nu_{hi}$ on the high-energy side remains unchanged; thus, the half-height bandwidth is calculated by [9]

$$\begin{aligned}\Delta v_{1/2}{}^{II} &= \Delta v_{hi} + (\lambda - 2H_{ab}) \\ &= [4\ln(2)\lambda RT]^{1/2} + (\lambda - 2H_{ab})\end{aligned} \tag{1.48c}$$

In the Class II–III limit ($2H_{ab} = \lambda$), or the borderline Class III [9], a half-cutoff at $2H_{ab}$ is expected, and then

$$\Delta V_{1/2}{}^{II-III} = [4\ln(2)\lambda RT]^{1/2} \tag{1.49a}$$

After entering the Class III region, when $\lambda < 2H_{ab} < (\lambda + \Delta\nu_{1/2}/4)$, the half-height bandwidth is calculated by Eq. (1.49). In the case of Class III, Eq. 1.49b indicates a sharp IVCT band because $2H_{ab} > \lambda$, which makes the $\Delta\nu_{1/2}{}^{III} < \Delta\nu_{hi}$ (=$[4\ln(2)\lambda RT]^{1/2}$). For very strongly coupled Class III systems, the bandwidth is given by

$$\Delta\boldsymbol{\nu}_{I/2}{}^{III} = -(2H_{ab} - \lambda) + \left[(2H_{ab} - \lambda)^2 + 4\ln(2)\lambda RT\right]^{1/2} \tag{1.49b}$$

Figure 1.6 shows the IVCT band shapes for MV compounds in different regimes of mixed valency [9, 10, 57]. Note that intensity cutoff caused by strong coupling is usually rounded off so that the band profile may not show clearly where it is being cut off as predicted. In the extreme of strong coupling, i.e. $2H_{ab}/\lambda \gg 1$, the "IVCT" band arises from electronic transition between the bonding and antibonding molecular orbitals. Thus, the dipole transition is more electronic but less vibronic in character; therefore, the observed absorption is narrow but more symmetric. This might be

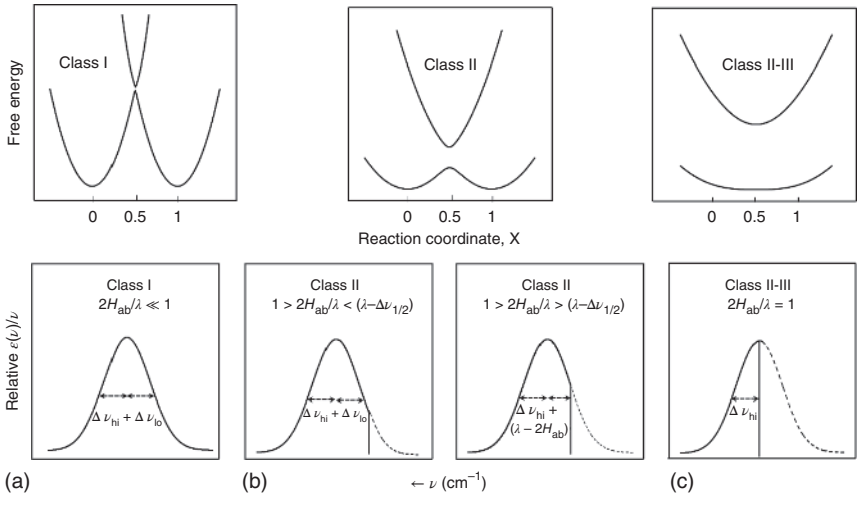

Figure 1.6 Adiabatic potential energy surfaces (top) and IVCT band shape predictions (bottom) for symmetric MV D-B-A compounds in Robin-Day's classification (a, Class I; b, Class II; c, Class III) from the two-state treatment.

thought of being the extreme of delocalization, for which treatment of the two-state model is no longer appropriate and Robin–Day's classification is inapplicable.

1.6.7 Rate Constant Expressions of Electron Transfer Reaction – The Marcus Theory

In the classical formalism, the reaction kinetics for thermal electron transfer (electron self-exchange) in D–B–A mixed-valence compounds are usually described by the transition-state theoretic model (TST). The transition state of electron transfer occurs at the crossing between the reactant and product diabatic states, or at the avoided region in the adiabatic potential surfaces, thus, at $X = 0.5$. In this situation, the ET reaction is governed by first-order kinetics. Therefore, the rate constant may be represented as [7]

$$k_{ET} = (\nu_n \kappa_{el})\kappa_n \tag{1.50}$$

where ν_n is the effective nuclear frequency, κ_{el} is the electronic transmission factor, and κ_n is the nuclear factor. In Eq. (1.50), κ_n represents the effective fraction of the reactant species in the transition state, while the fraction of the systems that successfully pass through the crossing region and on to the products per unit time is given by the product of ν_n and κ_{el}. For classical nuclear motion,

$$\kappa_n = \exp(-\Delta G^*/k_B T) \tag{1.51}$$

where k_B is the Boltzmann constant and ΔG^* the activation energy or the energy barrier for electron transfer. Then, the ET rate can be expressed by [122]

$$k_{ET} = \upsilon_n \kappa_{el} \exp(-\Delta G^*/k_B T) \tag{1.52}$$

in accordance with the familiar Arrhenius equation with the prefactor equaling $(\nu_n \kappa_{el})$. For thermal ET in solution, ν_n is controlled by the low-frequency vibrational modes (stretching, rotation, and translation) of the solvent molecules with a time scale of 1 – 10 ps, i.e. $10^{-12} - 10^{-13}$ seconds. Usually, an average nuclear frequency $\nu_n = 5 \times 10^{12}\ s^{-1}$ is adopted for determination of k_{ET} [6].

In the zero or weakly coupling situation, the system (Class I) can be treated in the nonadiabatic limit. Electron exchange between D and A occurs by crossing the diabatic intersection with energy barrier determined by Eq. (1.15) in the Marcus theory; for symmetric system ($\Delta G^0 = 0$), $\Delta G^* = \lambda/4$. However, the electronic transmission coefficient is very low, that is, $\kappa_{el} << 1$, because there is a small probability that the fraction of the reactant species in the transition state crosses the intersection, becoming the product. Adiabatic potential surfaces evolve with increasing the electronic coupling of the system. As a result, the thermal exchange barrier is lowered by the splitting between the upper and lower curves, i.e. $2H_{ab}$. In the adiabatic limit, ΔG^* is calculated from Eq. (1.29) for symmetric systems ($\Delta G^0 = 0$) or Eq. (1.30) for asymmetrical systems ($\Delta G^0 \neq 0$), both of which include contribution of H_{ab}. In this scenario, $\kappa_{el} \approx 1$ because nearly all the reactant species that reach the transition state are able to smoothly pass on to the product. Then, Eq. (1.53) is applied with the

prefactor $(\nu_n \kappa_{el}) = \nu_n$ by assuming $\kappa_{el} = 1$. This adiabatic treatment is applicable for Class II MV systems in a broad range of coupling strength, which are characterized by solvent-controlled electron transfer kinetics.

In condensed phase, electron transfer kinetics is governed by the interplay of the atomic (nuclear) and electronic dynamics of the system (including medium). Comparison between the electron hopping frequency (ν_{el}) and nuclear vibrational frequency (ν_n) determines ET in the adiabatic and nonadiabatic limits, that is

$$\text{adiabatic}: \nu_{el} >> \nu_n; \text{nonadiabatic}: \nu_{el} << \nu_n$$

while ν_n is averaged by the solvent modes and ν_{el} is a reflection of the joint influence of physical parameters H_{ab}, λ, and T, as indicated by [7, 19, 41, 64, 122]

$$\nu_{el} = \frac{2H_{ab}^2}{h}\sqrt{\frac{\pi^3}{\lambda k_B T}} \tag{1.53}$$

Semiclassical Landau–Zener models deal with the weakly coupled intermediate systems in the near-adiabatic regime, in which electron transfer crossing the intersection through nonadiabatic transition [19]. To quantitatively distinguish the nonadiabatic and adiabatic limits, the Landau–Zener models [111, 112] define two parameters: adiabatic parameter γ (Eq. 1.54a) and transition probability P_0 (Eq. 1.54b) with the exponent term being the nonadiabatic transition contribution, which gives the electronic transmission coefficient κ_{el} from Eq. (1.54c).

$$\gamma = \frac{H_{ab}^2}{2h\nu_n}\sqrt{\frac{\pi}{\lambda k_B T}} \tag{1.54a}$$

$$P_0 = 1 - \exp(-2\pi\gamma) \tag{1.54b}$$

$$\kappa_{el} = 2P_0/(1 + P_0) \tag{1.54c}$$

When $\gamma \gg 1$, the adiabatic limit is realized, and for thermal ET, $\kappa_{el} \approx 1$, while the nonadiabatic limit prevails with $\gamma \ll 1$. By definition of γ, it is clear that nonadiabatic transition is governed by the electronic and nuclear factors, represented by H_{ab} and ν_n, respectively.

In the nonadiabatic limit, as characterized by $\nu_{el} << \nu_n$, the electron hopping frequency (ν_{el}) dominates the ET process, and Eq. (1.52) is replaced by Eq. (1.55a)

$$k_{ET} = \upsilon_{el} \exp(-\Delta G^*/k_B T) \tag{1.55a}$$

The ET rate constant can be calculated by the Levich–Dogonadze–Marcus expression (Eq. 1.55b) [13, 38, 41]

$$k_{et} = \frac{2H_{ab}^2}{h}\sqrt{\frac{\pi^3}{\lambda k_B T}} \exp\left(-\frac{\lambda}{4k_B T}\right) \tag{1.55b}$$

Recent study [64] on MV complex system shows that both nonadiabatic (Eq. 1.55b) and adiabatic (Eq. 1.53) expressions work equally well for the intermediate systems.

1.6.8 McConnell Superexchange Mechanism and the CNS Model

Superexchange model has been widely accepted for interpretation of bridge-mediated electronic coupling and electron transfer through orbital interactions. It was first proposed by McConnell based on the simple two-state, one-electron approximation [16]. In McConnell's approach, the donor (ϕ_d) and acceptor (ϕ_a) states are separated by a bridge possessing n equivalent localized states ϕ_n. By neglecting direct donor–acceptor interactions, two new states ψ_S (symmetrical) and ψ_A (antisymmetrical) involving only the localized donor and acceptor states are formed

$$\psi_S = 1/\sqrt{2}(\phi_d + \phi_a) \tag{1.56a}$$

$$\psi_A = 1/\sqrt{2}(\phi_d - \phi_a) \tag{1.56b}$$

Here, the D–A coupling (H_{ab}) is small and neglectable, and other direct Hamiltonian matrix elements are zero by construction. However, the two states ϕ_d and ϕ_a interact with the nearest bridge states, and two nearest neighboring bridge states are allowed to interact with each other [16, 19]. Consequently, the degeneracy of ψ_S and ψ_A is removed, yielding an energy gap ΔE between them.

$$\Delta E = E_S + E_A = 2\sum_{n=1}^{n} \frac{\langle \phi_d \mid \boldsymbol{H} \mid \psi_n \rangle \langle \psi_n \mid \boldsymbol{H} \phi_a \rangle}{E_1 - E_n} \tag{1.57a}$$

where ψ_n and E_n are the eigenfunctions and eigenvalue of the nth unit in bridge block, which are identical for all units of the bridge. Mathematic treatments of Eq. (1.57a) with appropriate assumptions give rise to the McConnell superexchange expression (Eq. 1.57b) [19].

$$\Delta E = -(2T^2/E_{CT})(-t/E_{CT})^{n-1} \tag{1.57b}$$

where T is the matrix element accounting for the coupling between the donor and the first bridge unit ($n = 1$) or between the last bridge unit (n) and the acceptor, t is the matrix element that concerns the coupling between two neighboring bridge units, and E_{CT} is the energy difference between the donor (or acceptor) and bridge states [16].

It should be noted that the McConnell superexchange expression was derived originally in the nonadiabatic limit where the donor–acceptor coupling is extremely weak, by working on the example α,ω-diphenylalkanes [16]. Since there are no low-lying bridge orbitals available, involvement of virtual high-lying orbitals, for example, 3d orbitals of the sp^3 C chain, is assumed. However, the superexchange concept and expression (Eq. 1.57b) work equally well for transition metal and pure organic mixed-valence compounds with conjugated bridges. In these systems, the low-lying empty π* and high-lying filled π orbitals are exploitable, which provide the superexchange pathways for effective electron and hole transfer, respectively. Extended application of the McConnell equations is justified by the theoretic work from Reimers and Hush in 1994 [123], which demonstrated that the superexchange mechanism is appropriate for σ- or π-bonding bridged donor–acceptor systems

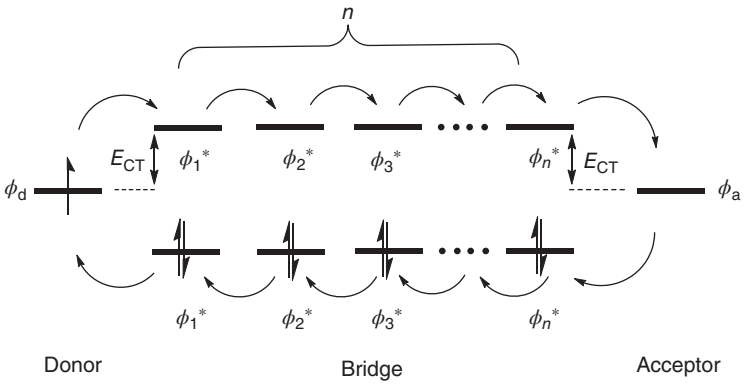

Figure 1.7 Schematic illustration of superexchange mechanism for bridge-mediated through-bond electron transfer. Electron transfer proceeds from the donor to the acceptor (from left to right) by the high-lying unoccupied bridge orbitals and hole transfer takes place through low-lying filled bridge orbitals.

in both resonant and near-resonant situations. The superexchange mechanism for long-distance through-bond electron transfer is schematically described in Figure 1.7. As a result of increasing the electronic coupling, the charge transfer system turns to be adiabatic. This is generally achieved by introducing conjugated bridge and reducing the number bridge units (n). In the adiabatic limit, Eq. (1.57a) gives $\Delta E = 2H_{ab}$, in accordance with $2H_{ab}/\lambda = 1$ from the semiclassical two-state model for the borderline Class II–III and Class III limit.

Superexchange and sequential electron (hole) hopping are the two pathways for electron transfer in the adiabatic and nonadiabatic limits, respectively. The former interprets the efficient mediation of bridge across a short distant by providing energy- and symmetry-compatible orbitals, while the latter has received broad success in interpretation of long-distance electron transfer. However, detailed investigations demonstrated that these two ET mechanisms may not be alternative but are combined or mixed to different extents [91, 124]. According to Eq. (1.57) and Figure 1.7, both pathways are conceptually the same in terms of orbital interactions. These two pathways are frequently characterized by an exponential decay parameter β that describes the different distance dependence of the coupling constant (H_{ab}), which gives exponential correlation of electron transfer rate constant k_{ET} with distance. From Eq. (1.57), letting $\beta r_{ab} = (n-1)$, we have Eq. (1.58)

$$H_{ab} = H_{ab}^0 \exp\left(-\frac{\beta}{2} r_{ab}\right) \tag{1.58}$$

where $H^0{}_{ab}$ is the electronic coupling at direct contact distance between the donor and acceptor [121]. The β value is expected to vary with the donor (acceptor)-bridge energy gap as well as with the coupling strength between the neighboring units of the bridge. When the subunit couplings are small compared to the energy gap (E_{CT}), from Eq. (1.57b), β is approximated by

$$\beta = \frac{2}{r_0} \ln\left(\frac{E_{CT}}{t}\right) \tag{1.59}$$

where r_0 is the length of one subunit [125]. For a given system, a larger value of β is found in the superexchange region, but a smaller β (weak distance dependence) is found for the sequential hopping mechanism. Ideally, for the series of MV compounds with a homologous bridge, an appreciable mechanistic transition can be probed by change of the β value with stepwise increasing the bridge length or the number of bridging units.

The McConnell superexchange formalism of ET has led Creutz, Newton, and Sutin to develop an alternative method to calculate the metal–metal coupling element $H_{MM'}$ for mixed-valence complexes M–BL–M′, known as the CNS model [10, 25, 116]. Following the same principle applied in development of the superexchange expression (Eq. 1.57b) [16, 19], CNS proposed calculation of $H_{MM'}$ from the metal–ligand (H_{ML} and $H_{M'L}$) and ligand–metal (H_{LM} and $H_{LM'}$) coupling elements by Eq. (1.60a).

$$H_{MM'} = \frac{H_{ML}H_{M'L}}{2\Delta E_{ML}} + \frac{H_{LM}H_{LM'}}{2\Delta E_{LM}} \tag{1.60a}$$

where the metal–ligand coupling elements are calculated from the Mulliken–Hush expression (Eq. 1.1) and the effective metal–ligand energy gap (ΔE_{ML}) and the effective ligand–metal energy gap (ΔE_{LM}) are calculated from Eq. (1.60b) and Eq. (1.60c), respectively.

$$\frac{1}{\Delta E_{ML}} = \frac{1}{2}\left(\frac{1}{\Delta E_{MLCT}}\right) + \left(\frac{1}{\Delta E_{MLCT} - \Delta E_{MM'CT}}\right) \tag{1.60b}$$

$$\frac{1}{\Delta E_{LM}} = \frac{1}{2}\left(\frac{1}{\Delta E_{LMCT}}\right) + \left(\frac{1}{\Delta E_{LMCT} - \Delta E_{MM'CT}}\right) \tag{1.60c}$$

In Eqs. (1.60b) and (1.60c), ΔE_{MLCT} and ΔE_{LMCT} are the measured MLCT and LMCT energies, respectively, from the electronic spectra of the singly reduced and oxidized mixed-valence compound, respectively, and $\Delta E_{MM'CT}$ refers to the IVCT transition energy (E_{IT}). The physical implication of the CNS model (Eq. 1.60) is that electron transfer and hole transfer pathways may be superpositioned, mutually contributing to the thermal electron exchange reaction. However, in application, one of the two pathways may be dominant over the other, depending on electronic structure of the bridge. Then, $H_{MM'}$ may be determined by one term of the two in Eq. (1.60a), for which mixing of metal center with ligand states is pronounced. Provided with electronically well-defined MV systems that permit accurate optical analysis, the H_{ab} values determined from the CNS model are in good agreement with the data from the Mulliken–Hush expression [68]. For weakly coupled $[\{Ru^{II}(NH_3)_5\}(\mu\text{-}4,4'\text{-bpy})\{Ru^{III}(NH_3)_5\}]^{5+}$, $H_{ab} = 900\,cm^{-1}$ is comparable with $H_{MM'} = 800\,cm^{-1}$ [25]. In the Mo_2–BL–Mo_2 mixed-valence systems, similar $H_{MM'}$ and H_{ab} values were found [63, 126].

1.7 Conclusion and Outlook

Mixed-valence chemistry was considered to be a ramification of inorganic chemistry half century ago when it was first introduced. Now, it expands into a huge body of molecular systems with the redox centers involving inorganic, organometallic, and pure organic units or groups linked by diverse chemical moieties. Research endeavor of decades has validated and resolved, to a large extent, the fundamental issues of mixed valency, typically, the physical origin of coloration of MV compounds, classification of MV classes, transition between the classes and ET energetics and kinetics, based on the semiclassical two-state and vibronic theories. However, these issues in MV chemistry concern electronic and nuclear degrees of freedom and the interplay between them, spreading far beyond the redox and spectroscopic properties presented by these molecules, but nearly every aspect of molecular science. Particularly, MV compounds, with the molecules in form of D–B–A as the prototype of study, are the excellent experimental models for which conventional spectral methods can be used advantageously to probe the electronic states and to monitor the vibronic dynamics. In this context, the wealth of knowledge of MV compounds has deepened our understanding of chemistry in general, and in particular, contributed to validation and refinement of the electron transfer theories.

Because of the broad interest and the specific concerns on electron transfer, MV chemistry will continue to serve an interplaying platform for both experimental and theoretical chemists who devote to gain new knowledge in this field. Given the controllable optical, electronic, and magnetic properties and great diversity in molecular assembly, MV compounds bear a great treasure of application potentials in the area of molecular optoelectronic and/or optomagnetic materials and devices. This should keep driving the study toward rational design and synthesis/fabrication of the functional molecular components and better microscopic understanding of the chemical principles. Elucidation of the functionalities of enzyme cofactors containing multiple metal centers in biological systems is the additional impetus of MV chemistry, which is helpful to development of biomimetic catalysts for solar energy conversion.

Acknowledgments

We thank the National Science Foundation of China (nos. 21971088, 20871093, 90922010, 21371074, and 21301070), the Natural Science Foundation of Guangdong Province (2018A030313894), and the Jinan University and Tongji University for financial support. We are grateful to Prof. Jeffrey Reimers (University of Technology Sydney), Prof. Yu-Wu Zhong (Institute of Chemistry, Chinese Academy of Sciences, Beijing), and Prof. Nathan J. Patmore (University of Huddersfield, UK) for their comments and suggestions on the manuscript.

References

1 Brown, D.B. (1980). *Mixed-Valence Compounds Theory and Applications in Chemistry, Physics, Geology, and Biology*. Dordrecht, Holland: D. Reidel Publishing Company.

2 Prassides, K. (1991). *Mixed Valency Systems: Applications in Chemistry*. Physics and Biology: Kluwer Academic Publishers.

3 Allen, G.C. and Hush, N.S. (1967). Intervalence-transfer absorption. Part 1. Qualitative evidence for intervalence-transfer absorption in inorganic systems in solution and in the solid state. *Prog. Inorg. Chem.* 8: 357–385.

4 Hansen, L.D., Litchman, W.M., and Daub, G.H. (1969). Turnbull's blue and Prussian blue: $KFe(III)[Fe(II)(CN)_6]$. *J. Chem. Educ.* 46: 46.

5 Hush, N.S. (1967). Intervalence-transfer absorption. II. theoretical considerations and spectroscopic data. *Prog. Inorg. Chem.* 8: 391–444.

6 Creutz, C. (1983). Mixed valence complexes of d^5-d^6 metal centers. *Prog. Inorg. Chem.* 30: 1–72.

7 Sutin, N. (1983). Theory of electron transfer reactions: insights and hindsights. *Prog. Inorg. Chem.* 30: 441–498.

8 Crutchley, R.J. (1994). Intervalence charge transfer and electron exchange studies of dinuclear ruthenium complexes. *Adv. Inorg. Chem.* 41: 273–325.

9 Brunschwig, B.S., Creutz, C., and Sutin, N. (2002). Optical transitions of symmetrical mixed-valence systems in the Class II–III transition regime. *Chem. Soc. Rev.* 31: 168–184.

10 D'Alessandro, D.M. and Keene, F.R. (2006). Current trends and future challenges in the experimental, theoretical and computational analysis of intervalence charge transfer (IVCT) transitions. *Chem. Soc. Rev.* 35: 424–440.

11 Kubo, R. and Toyozawa, Y. (1955). Application of the method of generating function to radiative and non-radiative transitions of a trapped electron in a crystal. *Prog. Theor. Phys.* 13: 160–182.

12 Levich, V.G. and Dogonadze, R.R. (1960). An adiabatic theory of electron processes in solutions. *Dokl. Akad. Nauk SSSR* 133: 158–161.

13 Levich, V.G. and Dogonadze, R.R. (1959). Theory of rediationless electron transitions between ions in solution. *Dokl Akad Nauk SSSR Ser Fiz Khim.* 124: 23–126.

14 Marcus, R.A. (1956). On the theory of oxidation-reduction reactions involving electron transfer. *I. J Chem. Phys.* 24: 966–978.

15 Marcus, R.A. (1957). On the theory of oxidation-reduction reactions involving electron transfer. II. Applications to data on the rates of isotopic exchange reactions. *J Chem. Phys.* 24: 867–871.

16 McConnell, H.M. (1961). Intramolecular charge transfer in aromatic free radicals. *J. Chem. Phys.* 35: 508–515.

17 Hush, N.S. (1958). Adiabatic rate processes at electrodes. I. Energy-Charge Relationships. *J. Chem. Phys.* 28: 962–972.

18 Creutz, C. and Taube, H. (1969). A direct approach to measuring the Franck-Condon barrier to electron transfer between metal ions. *J. Am. Chem. Soc.* 91: 3988–3989.

19 Newton, M.D. (1991). Quantum chemical probes of electron-transfer kinetics: the nature of donor-acceptor interactions. *Chem. Rev.* 91: 767–792.

20 Barbara, P.F., Meyer, T.J., and Ratner, M.A. (1996). Contemporary issues in electron transfer research. *J. Phys. Chem.* 100: 13148–13168.

21 Creutz, C. and Taube, H. (1973). Binuclear complexes of ruthenium ammines. *J. Am. Chem. Soc.* 95: 1086–1094.

22 Meyer, T.J. (1978). Optical and thermal electron transfer in metal complexes. *Acc. Chem. Res.* 11: 94–100.

23 Kaim, W. and Lahiri, G.K. (2007). Unconventional mixed-valent complexes of ruthenium and osmium. *Angew. Chem. Int. Ed.* 46: 1778–1796.

24 Heckmann, A. and Lambert, C. (2012). Organic mixed-valence compounds: a playground for electrons and holes. *Angew. Chem. Int. Ed.* 51: 326–392.

25 Brunschwig, B.S. and Sutin, N. (1999). Energy surfaces, reorganization energies, and coupling elements in electron transfer. *Coord. Chem. Rev.* 187: 233–254.

26 Newton, M.D. (2003). Thermal and optical electron transfer involving transition metal complexes: insights from theory and computation. *Coordin. Chem. Rev.* 238: 167–185.

27 Elliott, C.M., Derr, D.L., Matyushov, D.V., and Newton, M.D. (1998). Direct experimental comparison of the theories of thermal and optical electron-transfer: studies of a mixed-valence dinuclear iron polypyridyl complex. *J. Am. Chem. Soc.* 120: 11714–11726.

28 MacCarthy, G.R. (1926). Iron-stained sands and clays. *J. Geol.* 34: 352–360.

29 Hofmann, K.A. and Höschsele, K. (1915). Das Magnesiumchlorid als Mineralisator. II.: Das Urancerblau und das Wesen der konstitutiven Färbung. *Das Magnesiarot und das Magnesiagrün. K.* 48: 20–28.

30 Weyl, W.A. (1951). Light absorption as a result of an interaction of two states of valency of the same element. *J. Phys. Chem.* 55: 507–512.

31 Umena, Y., Kawakami, K., Shen, J.R., and Kamiya, N. (2011). Crystal structure of oxygen-evolving photosystem II at a resolution of 1.9 Å. *Nature* 473: 55–60.

32 Carrillo, N. and Ceccarelli, E.A. (2003). Open questions in ferredoxin-NADP+ reductase catalytic mechanism. *Eur. J. Biochem.* 270: 1900–1915.

33 Listorti, A., Durrant, J., and Barber, J. (2009). Solar to fuel. *Nature Mater.* 8: 929–930.

34 Robin, M.B. and Day, P. (1968). Mixed valence chemistry-a survey and classification. *Adv. Inorg. Chem. Radiochem.* 9: 247–422.

35 Creutz, C. and Taube, H. (1969). Direct approach to measuring the Franck-Condon barrier to electron transfer between metal ions. *J. Am. Chem. Soc.* 91: 3988–3989.

36 Mulliken, R.S. (1950). Structures of complexes formed by halogen molecules with aromatic and with oxygenated solvents. *J. Am. Chem.Soc.* 72: 600–608.

37 Mulliken, R.S. (1952). Molecular compounds and their spectra. III. The interaction of electron donors and acceptors. *J. Phys. Chem.* 56: 801–822.

38 Marcus, R.A. and Sutin, N. (1985). Electron transfers in chemistry and biology. *Biochim. Biophys. Acta* 811: 265–322.

39 Concepcion, J.J., Dattelbaum, D.M., Meyer, T.J., and Rocha, R.C. (2008). Probing the localized-to-delocalized transition. *Phil. Trans. R. Soc.* A366: 163–175.

40 Demadis, K.D., Hartshorn, C.M., and Meyer, T.J. (2001). The localized-to-delocalized transition in mixed-valence chemistry. *Chem. Rev.* 101: 2655–2685.

41 Levich, V.G. (1966). Present state of the theory of oxidation-reduction in solution (bulk and electrode reactions). *Adv. Electrochem. Electrochem. Eng.* 4: 249–371.

42 Dowling, N., Henry, P.M., Lewis, N.A., and Taube, H. (1981). Heteronuclear mixed-valence ions containing ruthenium and ferrocene centers. *Inorg. Chem.* 20: 2345–2348.

43 Hage, R., Haasnoot, J.G., Nieuwenhuis, H.A. et al. (1990). Synthesis, X-ray structure, and spectroscopic and electrochemical properties of novel heteronuclear ruthenium-osmium complexes with an asymmetric triazolate bridge. *J. Am. Chem. Soc.* 112: 9245–9251.

44 Zhong, Y.W., Gong, Z.L., Shao, J.Y., and Yao, J. (2016). Electronic coupling in cyclometalated ruthenium complexes. *Coord. Chem. Rev.* 312: 22–40.

45 Patoux, C., Launay, J.-P., Beley, M. et al. (1998). Long-range electronic coupling in bis(cyclometalated) ruthenium complexes. *J. Am. Chem. Soc.* 120: 3717–3725.

46 Cowan, D.O., LeVanda, C., Park, J., and Kaufman, F. (1973). Organic solid state. VIII. Mixed-valence ferrocene chemistry. *Acc. Chem. Res.* 6: 1–7.

47 Ribou, A.C., Launay, J.P., Sachtleben, M.L. et al. (1996). Intervalence electron transfer in mixed valence diferrocenylpolyenes. Decay law of the metal−metal coupling with distance. *Inorg. Chem.* 35: 3735–3740.

48 Bruns, W. and Kaim, W. (1990). Bindungscharakteristik der H,-koordinierenden Fragmente $W(CO)_3(PR_3)_2$.Aussergewiihnliche optische und elektrochemische Eigenschaften zweikerniger Pyrazinkomplexe. *J. Organomet. Chem.* 390: C45–C49.

49 Bruns, W., Kaim, W., Waldhör, E., and Krejčik, M. (1993). Spectroelectrochemical characterization of a pyrazine-bridged mixed-valent ($4d^5/4d^6$) organometallic analogue of the Creutz–Taube ion. *Chem. Commun.* 24: 1868–1869.

50 NavasáBadiola, J.A. and Michael, D. (1993). Metal–metal interactions across symmetrical bipyridyl bridging ligands in binuclear seventeen-electron molybdenum complexes. *J. Chem. Soc. Dalton.* 5: 681–686.

51 Ward, M.D. (1995). Metal-metal interactions in binuclear complexes exhibiting mixed valency; molecular wires and switches. *Chem. Soc. Rev.* 24: 121–134.

52 Bonvoisin, J., Launay, J.P., Vanderauweraer, M., and Deschryver, F.C. (1994). Organic mixed-valence systems-intervalence transition in partly oxidized aromatic polyamines-electrochemical and optical studies. *J. Phys. Chem. C* 98: 5052–5057.

53 Lambert, C. and Nöll, G. (1999). The class II/III transition in triarylamine redox systems. *J. Am. Chem. Soc.* 121: 8434–8442.

54 Nelsen, S.F., Ismagilov, R.F., and Powell, D.R. (1996). Charge localization in a dihydrazine analogue of tetramethyl-p-phenylenediamine radical cation. *J. Am. Chem. Soc.* 118: 6313–6314.

55 Nelsen, S.F., Ismagilov, R.F., and Trieber, D.A. (1997). Adiabatic electron transfer: comparison of modified theory with experiment. *Science* 278: 846–849.

56 Lindeman, S.V., Rosokha, S.V., Sun, D., and Kochi, J.K. (2002). X-ray structure analysis and the intervalent electron transfer in organic mixed-valence crystals with bridged aromatic cation radicals. *J. Am. Chem. Soc.* 124: 843–855.

57 Nelsen, S.F. (2000). "Almost delocalized" intervalence compounds. *Chem. Eur. J.* 6: 581–588.

58 Cayton, R.H. and Chisholm, M.H. (1989). Electronic coupling between covalently linked metal-metal quadruple bonds of molybdenum and tungsten. *J. Am. Chem. Soc.* 111: 8921–8923.

59 Cayton, R.H., Chisholm, M.H., Huffman, J.C., and Lobkovsky, E.B. (1991). Metal-metal multiple bonds in ordered assemblies. 1. Tetranuclear molybdenum and tungsten carboxylates involving covalently linked metal-metal quadruple bonds. Molecular models for subunits of one-dimensional stiff-chain polymers. *J. Am. Chem. Soc.* 113: 8709–8724.

60 Cotton, F.A., Donahue, J.P., Murillo, C.A., and Pérez, L.M. (2003). Polyunsaturated dicarboxylate tethers connecting dimolybdenum redox and chromophoric centers: absorption spectra and electronic structures. *J. Am. Chem. Soc.* 125: 5486–5492.

61 Cotton, F.A., Liu, C.Y., Murillo, C.A. et al. (2004). Strong electronic coupling between dimolybdenum units linked by the N, N′-dimethyloxamidate anion in a molecule having a heteronaphthalene-like structure. *J. Am. Chem. Soc.* 126: 14822–14831.

62 Cotton, F.A., Murillo, C.A., and Walton, R.A. (2005). Introduction and survey. In: *Multiple Bonds Between Metal Atoms* (ed. F.A. Cotton, C.A. Murillo and R.A. Walton), 1–21. Boston, MA: Springer.

63 Liu, C.Y., Xiao, X., Meng, M. et al. (2013). Spectroscopic study of δ electron transfer between two covalently bonded dimolybdenum units via a conjugated bridge: adequate complex models to test the existing theories for electronic coupling. *J. Phys. Chem. C.* 117: 19859–19865.

64 Zhu, G.Y., Qin, Y., Meng, M. et al. (2021). Crossover between the adiabatic and nonadiabatic electron transfer limits in the Landau-Zener model. *Nat. Commun.* 12 (456): 1–10.

65 Xu, G.L., Zou, G., Ni, Y.H. et al. (2003). Polyyn-diyls capped by diruthenium termini: a new family of carbon-rich organometallic compounds and distance-dependent electronic coupling therein. *J. Am. Chem. Soc.* 125: 10057–10065.

66 Ito, T., Hamaguchi, T., Nagino, H. et al. (1999). Electron transfer on the infrared vibrational time scale in the mixed valence state of 1,4-pyrazine- and 4,4'-bipyridine-bridged ruthenium cluster complexes. *J. Am. Chem. Soc.* 121: 4625–4632.

67 Ito, T., Hamaguchi, T., Nagino, H. et al. (1997). Effects of rapid intramolecular electron transfer on vibrational spectra. *Science* 277: 660–663.

68 Rosokha, S.V., Sun, D.-L., and Kochi, J.K. (2002). Conformation, distance, and connectivity effects on intramolecular electron transfer between phenylene-bridged aromatic redox centers. *J. Phys. Chem. A.* 106: 2283–2292.

69 Launay, J.-P. (2001). Long-distance intervalence electron transfer. *Chem. Soc. Rev.* 30: 386–397.

70 Chen, H.W., Mallick, S., Zou, S.F. et al. (2018). Mapping bridge conformational effects on electronic coupling in Mo_2–Mo_2 mixed-valence systems. *Inorg. Chem.* 57: 7455–7467.

71 Bursten, B.E., Chisholm, M.H., Clark, R.J. et al. (2002). Perfluoroterephthalate bridged complexes with M– M quadruple bonds:(t-$BuCO_2)_3M_2(\mu$-$O_2CC_6F_4CO_2)$ $M_2(O_2CtBu)_3$, where M= Mo or W. Studies of solid-state, molecular, and electronic structure and correlations with electronic and Raman spectral data. *J. Am. Chem. Soc.* 124: 12244–12254.

72 Nelsen, S.F., Konradsson, A.E., and Teki, Y. (2006). Charge-localized naphthalene-bridged bis-hydrazine radical cations. *J. Am. Chem. Soc.* 128: 2902–2910.

73 Kaliginedi, V., Moreno-García, P., Valkenier, H. et al. (2012). Correlations between molecular structure and single-junction conductance: a case study with oligo (phenylene-ethynylene)-type wires. *J. Am. Chem. Soc.* 134: 5262–5275.

74 Venkataraman, L., Klare, J.E., Nuckolls, C. et al. (2006). Dependence of single-molecule junction conductance on molecular conformation. *Nature* 442: 904–907.

75 Gao, H., Mallick, S., Cao, L. et al. (2019). Electronic coupling and electron transfer between two Mo_2 units through meta-and para-phenylene bridges. *Chem. Eur. J.* 25: 3930–3938.

76 Forrest, W.P., Choudhuri, M.M., Kilyanek, S.M. et al. (2015). Synthesis and electronic structure of Ru_2(X*ap*)$_4$(Y-*gem*-DEE) type compounds: effect of cross-conjugation. *Inorg. Chem.* 54: 7645–7652.

77 Göransson, E., Emanuelsson, R., Jorner, K. et al. (2013). Charge transfer through cross-hyperconjugated versus cross-π-conjugated bridges: an intervalence charge transfer study. *Chem. Sci.* 4: 3522–3532.

78 Cheng, T., Shen, D.X., Meng, M. et al. (2019). Efficient electron transfer across hydrogen bond interfaces by proton-coupled and-uncoupled pathways. *Nat. Commun.* 10 (1053): 1–10.

79 Tadokoro, M., Inoue, T., Tamaki, S. et al. (2007). Mixed-valence states stabilized by proton transfer in a hydrogen-bonded biimidazolate rhenium dimer. *Angew. Chem. Int. Ed.* 119: 6042–6046.

80 Wilkinson, L.A., Vincent, K.B., Meijer, A.J., and Patmore, N.J. (2016). Mechanistic insight into proton-coupled mixed valency. *Chem. Commun.* 52: 100–103.

81 Sun, H., Steeb, J., and Kaifer, A.E. (2006). Efficient electronic communication between two identical ferrocene centers in a hydrogen-bonded dimer. *J. Am. Chem. Soc.* 128: 2820–2821.

82 Ghaddar, T.H., Castner, E.W., and Isied, S.S. (2000). Molecular recognition and electron transfer acrossa hydrogen bonding interface. *J. Am. Chem. Soc.* 122: 1233–1234.

83 Hammes-Schiffer, S. and Stuchebrukhov, A.A. (2010). Theory of coupled electron and proton transfer reactions. *Chem. Rev.* 110: 6939–6960.

84 Liu, Y., Lagrost, C., Costuas, K. et al. (2008). A multifunctional organometallic switch with carbon-rich ruthenium and diarylethene units. *Chem. Commun.* 46: 6117–6119.

85 Chisholm, M.H., Feil, F., Hadad, C.M., and Patmore, N.J. (2005). Electronically coupled MM quadruply-bonded complexes (M= Mo or W) employing functionalized terephthalate bridges: toward molecular rheostats and switches. *J. Am. Chem. Soc.* 127: 18150–18158.

86 Wenger, O.S. (2012). Photoswitchable mixed valence. *Chem. Soc. Rev.* 2012 (41): 3772–3779.

87 Peloquin, J.M., David Britt, R., Peloquin, J.M., and Britt, R.D. (2001). EPR/ENDOR characterization of the physical and electronic structure of the OEC Mn cluster Biochim. *Biophys. Acta* 1503: 96–111.

88 Zhang, C., Chen, C., Dong, H. et al. (2015). A synthetic Mn4Ca-cluster mimicking the oxygen-evolving center of photosynthesis. *Science* 348: 690–693.

89 Nelsen, S.F., Ismagilov, R.F., and Powel, D.R. (1997). Charge-localized p-phenylenedihydrazine radical cations: ESR and optical studies of intramolecular electron transfer rates. *J. Am. Chem. Soc.* 119: 10213–10222.

90 Chisholm, M.H., Pate, B.D., Wilson, P.J., and Zaleski, J.M. (2002). On the electron delocalization in the radical cations formed by oxidation of MM quadruple bonds linked by oxalate and perfluoroterephthalate bridges. *Chem. Commun.* 10: 1084–1085.

91 Lloveras, V., Vidal-Gancedo, J., Figueira-Duarte, T.M. et al. (2011). Tunneling versus hopping in mixed-valence oligo-p-phenylenevinylene polychlorinated bis (triphenylmethyl) radical anions. *J. Am. Chem. Soc.* 133: 5818–5833.

92 Lancaster, K., Odom, S.A., Jones, S.C. et al. (2009). Intramolecular electron-transfer rates in mixed-valence triarylamines: measurement by variable-temperature ESR spectroscopy and comparison with optical data. *J. Am. Chem. Soc.* 131: 1717–1723.

93 Richardson, D.E. and Taube, H. (1981). Determination of $E_2°$-$E_1°$ in multistep charge transfer by stationary-electrode pulse and cyclic voltammetry: application to binuclear ruthenium ammines. *Inorg. Chem.* 20: 1278–1285.

94 Evans, C.E., Naklicki, M.L., Rezvani, A.R. et al. (1998). An investigation of superexchange in dinuclear mixed-valence ruthenium complexes. *J. Am. Chem. Soc.* 120: 13096–13103.

95 Richardson, D.E. and Taube, H. (1984). Mixed-valence molecules: electronic delocalization and stabilization. *Coord. Chem. Rev.* 60: 107–129.

96 Low, P.J. and Brown, N.J. (2010). Electronic interactions between and through covalently bonded polymetallic complexes. *J. Clust. Sci.* 21: 235–278.

97 Hush, N.S. (1961). Adiabatic theory of outer sphere electron-transfer reactions in solution. *Trans. Faraday Soc.* 57: 557–580.

98 Marcus, R.A. (1964). Chemical and electrochemical electron transfer theory. *Annu. Rev. Phys. Cbem.* 15: 155–196.

99 Nelsen, S.F. and Newton, M.D. (2000). Estimation of electron transfer distances from AM1 calculations. *J. Phys. Chem. A* 104: 10023–10031.

100 Reimers, J.R. and Hush, N.S. (1991). Electronic properties of transition-metal complexes determined from electroabsorption (Stark) spectroscopy. 2. Mononuclear complexes of ruthenium(II). *J. Phys. Chem.* 95: 9773–9781.

101 Brunschwig, B.S., Creutz, C., and Sutin, N. (1998). Electroabsorption spectroscopy of charge transfer states of transition metal complexes. *Coord. Chem. Rev.* 177: 61–79.

102 Cheng, T., Tan, Y.N., Zhang, Y. et al. (2015). Distinguishing the strength of electronic coupling for Mo_2-containing mixed-valence compounds within the class III regime. *Chem. Eur. J.* 21: 2353–2357.

103 Tan, Y.N., Cheng, T., Meng, M. et al. (2017). Optical behaviors and electronic properties of Mo2–Mo2 mixed-valence complexes within or beyond the Class III regime: testing the limits of the two-state model. *J. Phys. Chem. C* 121: 27860–27873.

104 Lear, B.J. and Chisholm, M.H. (2009). Oxalate bridged MM (MM = Mo_2, MoW, and W_2) quadruply bonded complexes as test beds for current mixed valence theory: looking beyond the intervalence charge transfer transition. *Inorg. Chem.* 48: 10954–10971.

105 Wu, Y.Y., Meng, M., Wang, G.Y. et al. (2017). Optically probing the localized to delocalized transition in Mo_2–Mo_2 mixed-valence systems. *Chem. Comm.* 53: 3030–3033.

106 Lambert, C., Amthor, S., and Schelter, J. (2004). From valence trapped to valence delocalized by bridge state modification in bis (triarylamine) radical cations: evaluation of coupling matrix elements in a three-level system. *J. Phys. Chem. A* 108: 6474–6486.

107 Xiao, X., Liu, C.Y., He, Q. et al. (2013). Control of the charge distribution and modulation of the Class II–III transition in weakly coupled Mo_2–Mo_2 systems. *Inorg. Chem.* 52: 12624–12633.

108 Lear, B.J., Glover, S.D., Salsman, J.C. et al. (2007). Solvent dynamical control of ultrafast ground state electron transfer: implications for Class II–III mixed valency. *J. Am. Chem. Soc.* 129: 12772–12779.

109 Chen, P.Y. (1998). Medium effects on charge transfer in metal complexes. *Chem. Rev.* 98: 1439–1478.

110 Demadis, K.D., Neyhart, G.A., Kober, E.M. et al. (1999). Intervalence transfer at the localized-to-delocalized, mixed-valence transition in osmium polypyridyl complexes. *Inorg. Chem.* 38: 5948–5959.

111 Landau, L.D. (1932). Zur theorie der energieübertragung bei stössen. *Phys. Z. Sowjetunion* 1: 88–98.

112 Zener, C. (1932). Non-adiabatic crossing of energy levels. *Proc. R. Soc. Lond. A* 137: 696–702.

113 Marcus, R.A. (1960). Exchange reaction and electron transfer reactions including isotopic exchange. Theory of oxidation-reduction reactions involving electron transfer. *Disc. Faraday. Soc.* 29: 21–31.

114 Marcus, R.A. (1965). On the theory of electron transfer reactions. VI. Unified treatment for homogeneous and electrode Reactions. *J. Chem. Phys.* 43: 679–701.

115 Marcus, R.A. (1993). Electron transfer reactions in chemistry: theory and experiment. *Angew. Chem. Int. Ed. Engl.* 32: 1111–1121.

116 Creutz, C., Newton, M. D., Sutin, N. (1994). Metal-ligand and metal-metal coupling elements. *J. Photochem. Photobiol. A: Chem.*, 82, 47-59.

117 Wu, H.-Y., Ren, H.-S., Zhu, Q., and Li, X.-Y. (2012). A modified two-sphere model for solvent reorganization energy in electron transfer. *Phys. Chem. Chem. Phys.* 14: 5538–5544.

118 Li, X.-Y. (2015). An overview of continuum models for nonequilibrium solvation: popular theories and new challenge. *Int. J. Quantum Chem.* 115: 700–721.

119 Cave, R.J. and Newton, M.D. (1996). Generalization of the Mulliken-Hush treatment for the calculation of electron transfer matrix elements. *Chem. Phys. Lett.* 249: 15–19.

120 Silverman, L.N., Kanchanawong, P., Treynor, T.P., and Boxer, S.G. (2008). Stark spectroscopy of mixed-valence systems. *Phil. Trans. R. Soc. A* 366: 33–45.

121 Amthor, S. and Lambert, C. (2006). [2.2] Paracyclophane-bridged mixed-valence compounds: application of a generalized Mulliken-Hush three-level model. *J. Phys. Chem. A* 110: 1177–1189.

122 Newton, M.D. and Sutin, N. (1984). Electron transfer reactions in condensed phases. *Ann. Rev. Phys. Chem.* 35: 437–480.

123 Reimers, J.R. and Hush, N.S. (1994). Electron transfer and energy transfer through bridged systems III. Tight-binding linkages with zero or non-zero asymptotic band Gap. *J. Photochem. Photobiol. A: Chem.* 82: 31–46.

124 Lambert, C., Nöll, G., and Schelter, J. (2002). Bridge-mediated hopping or superexchange electron-transfer processes in bis (triarylamine) systems. *Nat. Mat.* 1: 69–73.

125 Eng, M.P. and Albinsson, B. (2006). Non-exponential distance dependence of bridge-mediated electronic coupling. *Angew. Chem. Int. Ed.* 45: 5626–5629.

126 Xiao, X., Meng, M., Lei, H., and Liu, C.Y. (2014). Electronic coupling and electron transfer between two dimolybdenum units spaced by a biphenylene group. *J. Phys. Chem. C* 118: 8308–8315.